BACHELOR

Random intersection graphs as a quantitative model for the Rydberg blockade effect

Rutten, Daan J.

Award date:
2018

Random intersection graphs as a quantitative model for the Rydberg blockade effect

Bachelor's thesis

Daan Rutten

Eindhoven, University of Technology
May 1, 2018

Abstract

If an atom in an ultracold Rydberg gas becomes excited, it can block neighbouring atoms from becoming excited due to strong dipole interactions. This Rydberg blockade effect causes the gas to end up in a state called the jamming limit in which each particle is either excited or blocked. The process of sequentially exciting a particle is an inherently complex mathematical problem due to the spatial correlations the blockade effect induces. In this thesis, random graphs are used to describe the Rydberg blockade effect. A novel type of random graph, the decomposed random intersection graph, is proposed which is capable of predicting the random sequential adsorption process several times better than existing analytical methods. Finally, although random graphs contain no explicit notion of the position of a vertex, two ways of implicitly measuring spatial correlations on random graphs are explored.

Preface

This thesis has been the most intellectually challenging project I have ever undertaken, it has turned out to be the project which I am most proud of and it feels like this project contains a piece of me, eternally captured in the same letters you are reading. During the countless hours I have spent working on this project, I have learned to love mathematics, and to hate it occasionally as well. I have learned the beauty of abstraction, of perseverance and finally of satisfaction.

To the reader, I want to issue a mild warning. This thesis is dense. Although most results can be interpreted intuitively, completely understanding all concepts requires careful and possibly repeated reading. I have deliberately tried to introduce the topics and processes with relatively simple, though important models in the first few chapters, gradually building towards more complicated models in later chapters. While it is not difficult to lose oneself in the equations presented, it is as important, if not more important, to grasp the ideas from which these equations follow. I sincerely hope you enjoy reading this thesis and I aspire to convey the same childlike curiosity I felt from exploring unknown territory.

I want to thank Souvik Dhara for his patience and extensive feedback, Servaas Kokkelmans for his contagious enthusiasm and his inclination to push even further and Debankur Mukherjee for his motivating support. Finally, I would like to thank Johan van Leeuwaarden for introducing me to the topic.

To my parents, who actually insisted to be mentioned is this preface, you are the most admirable, patient and loving parents I could ever hope for. Although I am afraid the contents of this thesis are still a mystery, you read it from front to back. Without you, I would never be the person I am now. I am grateful for every step of the way. Thank you.

Daan Rutten

Eindhoven, The Netherlands
May 1, 2018

Contents

1 Introduction

Due to their extravagant characteristics, Rydberg gases have been a frequent subject of research. Their applications for experimental physics include areas such as quantum computing and simulating quantum many-body physics. However, spatial behaviour of Rydberg atoms complicates mathematical analysis of processes on a Rydberg gas. A possible solution is to use random graphs for describing Rydberg atoms. The lack of spatial information in a random graph is essential for the feasibility of obtaining an analytical expression. This thesis researches the applicability of random intersection graphs as a model for the excitation of Rydberg atoms with the goal of improving the accuracy of existing methods. Random intersection graphs are favourable due to their ability of tuning both the mean degree of a vertex and the tendency of clustering.

Figure 1 introduces the different chapters in this thesis in a schematic overview. In chapter 2, properties of Rydberg gases are introduced together with the Rydberg blockade effect. The chapter sets the foundation for establishing the connection between Rydberg gases and random geometric graphs mainly referring to literature for detailed studies of the applicability of random geometric graphs as a model. Chapter 3 continues with a formal definition of random geometric graphs. The random sequential adsorption process on a graph is also explained leading to two fundamental theorems, a law of large numbers (LLN) and a central limit theorem (CLT) for the number of activated particles. The chapter concludes with results from simulations done on random geometric graphs. Chapter 4 provides an overview of previous research done on the connection between random graphs and the Rydberg blockade effect. In chapter 5 the random intersection graph is introduced. The chapter compares the graph to a random geometric graph on three properties. The LLN and CLT for random sequential adsorption on a random intersection graph are introduced for which chapter 9 provides a formal proof. Chapter 6 introduces a novel type of random graph which is a better predictor of the random sequential adsorption process. Finally, chapter 7 discusses two ways of extracting spatial information from random graphs.

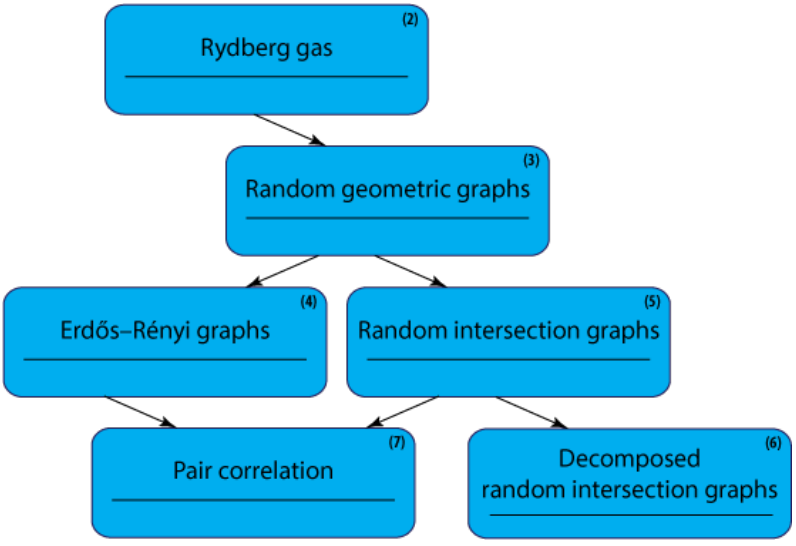

Figure 1: Overview of relationship between the different chapters in this thesis.

2 Rydberg gases

Nowadays Rydberg atoms are a frequent research subject in fundamental quantum research. Rydberg systems are attractive for use in experimental setups due to their exaggerated atomic properties. It has been proposed that Rydberg atoms can be used for implementing quantum gates due to their strong long-range interactions [1]. Moreover, other applications such as light-atom interfaces and simulating quantum many-body physics have been proposed as well [2]. In this chapter several properties of Rydberg atoms will be highlighted before focusing on the dipole blockade effect relevant for the continuation of this thesis.

2.1 Properties of Rydberg atoms

In general Rydberg atoms act as exaggerated versions of classical atoms. The following are properties of Rydberg atoms compared to classical atoms for a quantum number $n \sim 100$ [3].

1. Their size is $\sim 1\,\mu\text{m}$ while a typical atomic radius for classical atoms is $\sim 100\,\text{pm}$.
2. The binding energy is $\sim 300\,\text{GHz}$ compared to a binding energy of $\sim 3\,\text{PHz}$ for hydrogen. Furthermore, spin-orbit effects such as fine structure splitting are still present at large n.
3. Their radiative lifetime is $\sim 1\,\mu\text{s}$ while for hydrogen the radiative lifetime is $\sim 100\,\text{ns}$.
4. The elements in the dipole matrix are large ($\sim n^2$ Debye).
5. Rydberg atoms are very sensitive to electric fields.

These properties provide extensive benefits for use of Rydberg atoms in experimental setups. Due to their long radiative lifetime it is feasible to carry out measurements on Rydberg atoms while in their excited state. The radiative lifetime increases even more when n or l increases. Next, their large dipole moments allow for exploring many-body cooperations or collective effects at a macroscopic scale. Assembling a many-atomic sample could serve as a quantum simulator because the sample allows for fine-grained experimental control. Finally, a static electric field mixes the Rydberg states creating a permanent dipole moment. With an electric field the Rydberg-Rydberg interaction can therefore be tuned.

2.2 Dipole blockade effect

Consider a volume of an ultracold Rydberg gas. Each atom in this volume has a ground state $|g\rangle$ and a Rydberg state $|r\rangle$ separated by an energy E. If two atoms in the volume do not interact, each of the two atoms can be brought to their Rydberg state individually by a laser excitation. When looking at the two-atom system a transition from $|g,g\rangle$ to either $|g,r\rangle$ or $|r,g\rangle$ is possible at energy E, which can be followed by a transition to $|r,r\rangle$ also separated by an energy E. The state in which both atoms are in the Rydberg state can therefore be reached with laser excitations. In reality, however, two atoms in the volume do interact with each other due to strong dipole forces [4]. When two atoms are in the state $|r,r\rangle$ their dipole-dipole interaction creates an energy shift of $\Delta E = \pm\frac{C_3}{R^3}$, depending on the inter atomic distance R. The interaction is schematically shown in Figure 2.

When exciting an atom within an ultracold Rydberg gas to its excited state, the atom thus creates an energy shift influencing nearby atoms. When the energy shift is large enough, the laser is out of resonance with the $|r,r\rangle$ state and the dipole interaction blocks the second atom from transferring to the Rydberg state. This effect is called the dipole blockade effect or Rydberg blockade effect.

As the energy shift depends inversely on the inter atomic distance, the blockade effect occurs only for atoms which are close enough. The further the atoms are apart, the smaller the energy shift and the closer the highest energy level is to be within resonance of the laser. The profile of the laser determines which energy levels are still attainable and how likely the transition is. Combining these two factors yields Figure 3a, which shows a fictitious example of the probability

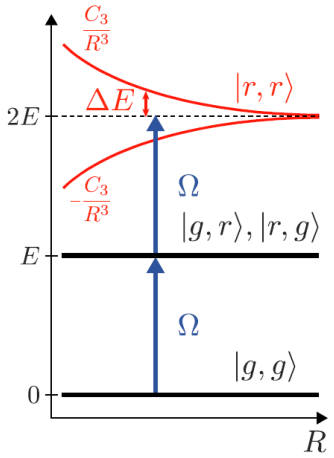

Figure 2: Energy shift of two atoms in the Rydberg state when separated by a distance R. Here Ω denotes the Rabi frequency of the coupled states $|g\rangle$ and $|r\rangle$ (from [4]).

of a laser excitation as a function of inter atomic distance. When the laser profile is sharp, the function can be estimated by the piecewise function

$$\mathbb{P}(v \text{ can be excited} \mid w \text{ excited}, d(v,w) = R) = \begin{cases} 0, & \text{if } R \leq R_b \\ 1, & \text{if } R > R_b \end{cases} \tag{2.1}$$

where R_b denotes the blockade radius. The distance between the atoms v and w is indicated by $d(v,w)$. Following this approximation, exciting an atom always blocks the atoms within a radius R_b around the atom. Atoms separated by a distance larger than R_b are unaffected by the excitation. This idea corresponds to the laser having a fixed range of energy levels which it can reach with equal probability. This range then determines the blockade radius as shown in Figure 3b. The applicability of this estimation has been researched closely and it has been found to be a proper description for systems consisting of three or even more atoms [5].

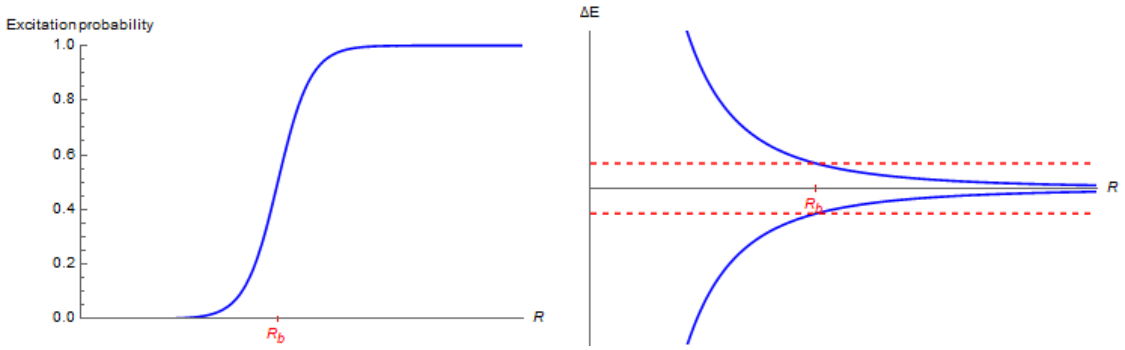

(a) (b)

Figure 3: Figure (a) shows the probability of a laser excitation as a function of inter atomic distance. Figure (b) shows the energy shift depending on the distance between two atoms. The range of reachable energy levels is illustrated by the dashed red lines. The blockade radius R_b is indicated in both figures.

What would happen if we try to excite each atom in the volume? After a while all possible excitations have occurred and the number of excitations will no longer increase, a state called the jamming limit. Not every atom is excited in the jamming limit because for some atoms the probability of excitation is zero depending on the inter atomic distance to an atom which

is already excited. This yields the question of how many excitations must take place before the jamming limit is reached. This quantity is often measured by the Mandel Q parameter, which is introduced in the next section. Also, spatial correlations of excited atoms have been observed in the jamming limit due to the blockade effect [6]. Hence, an interesting subject for research is finding a description for the spatial correlation of an ultracold Rydberg gas in the jamming limit.

2.3 Mandel Q parameter

Depict a setup involving an ultracold Rydberg gas of density ρ having volume V. The number of atoms N in the volume is inherently random and is assumed to follow a Poisson distribution. The temperature of an ultracold Rydberg gas is of the order of micro Kelvin such that the atoms within the volume are static. As the number of atoms in any volume is Poissonian, this implies that the atoms are uniformly distributed over the volume V. A laser facilitates the excitation of atoms to their Rydberg state until the jamming limit has been reached.

The Mandel Q parameter provides information about the number of excitations in the jamming limit. Denote the number of excited atoms in the jamming limit by X_∞. The number of excited particles is a random quantity because for every instance of a Rydberg gas the number of excited atoms can be different. The Mandel Q parameter is then characterized as follows [7].

$$Q = \frac{\mathrm{Var}(X_\infty)}{\mathbf{E}[\,X_\infty]} - 1 \tag{2.2}$$

When the number of excited particles follows a Poisson distribution, $Q = 0$. We will call the process sub-Poissonian whenever $Q < 0$ and super-Poissonian when $Q > 0$. For a Rydberg gas the number of excited particles is usually sub-Poissonian [8]. Hence, the ratio of the variance and the expected number of excitations is apparently smaller than one. Note that $Q = 0$ for a process in which there would be no Rydberg blockade effect because the total number of excitable particles is Poissonian. For small R_b the Mandel Q parameter must therefore be close to zero.

Finding an explicit expression for the Mandel Q parameter has proved to be hard. Although numerical techniques involving Dicke states are known [9], an exact closed formula has yet to be discovered. An attempt to obtain an analytical expression has been made by using Erdős–Rényi random graphs [10]. Their approach will be explained in chapter 4 as this thesis borrows the idea of using random graphs. The model in this thesis extends the idea of using random graphs and obtains a model which can achieve an even higher accuracy.

2.4 Pair correlation

As previously mentioned, interest has been shown in descriptions of the spatial behaviour of excitations in a Rydberg gas. A quantitative description of the spatial behaviour is represented by the pair correlation $g(R)$. Given a Rydberg gas in the jamming limit, the pair correlation is the normalized probability of two atoms being in their Rydberg state given that their distance is R as a function of R. Formally

$$g(R) = \lim_{\delta \to 0} \frac{\mathbb{P}(v, w \in \hat{X}_\infty \mid d(v,w) \in [R, R+\delta))}{\mathbb{P}(v \in \hat{X}_\infty)^2}, \tag{2.3}$$

where $\hat{X}_\infty$ is the set of excited atoms in the jamming limit. Figure 4 shows an example of the pair correlation as numerically calculated from the two-atom wave function [11]. If the two excitations were uncorrelated, the pair correlation would be one. For large distances the pair correlation indeed approaches one, which implies that excited particles do not influence each other at large distances. For distances smaller than the blockade radius the pair correlation is zero. Two atoms cannot be excited at the same time when their distance is less than the blockade radius due to their dipole interaction.

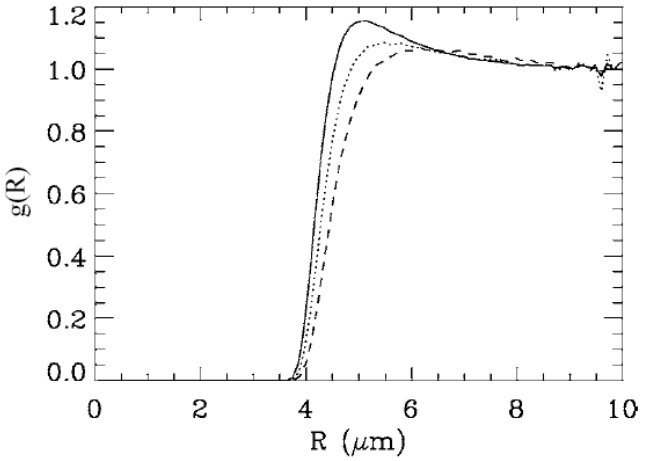

Figure 4: The pair correlation between Rydberg atoms as a function of distance for different laser amplitudes. The blockade radius is 3.7 µm (from [11]).

A noticeable feature of the pair correlation is the peak at a distance slightly larger than the blockade radius. The probability of having two excited atoms at this distance is larger than the probability of exciting two particles individually. Intuitively this is sensible. An optimal distribution of the excited particles over space would place each particle at the edge of the blockade sphere of a previous particle. The distribution is optimal in a sense that in this way the maximum number of excitations occurs. In a random process the spaces around the edges of the blockade sphere will thus be more often available compared to spaces favouring a less optimal distribution of excited atoms. Excitations at this distance are therefore more likely to happen.

It is important to realize the difference between the pair correlation and the function devised earlier in Figure 3a. The function devised earlier gives the probability that an excitation still *can* happen when a particle is a distance R apart from an already excited particle. The pair correlation on the other hand is a function only observable *after* the process of excitation is conducted and the jamming limit has been reached. It is defined as the normalized probability of finding two excited atoms at a certain distance. This can include more complex interactions between excitations which for example explain the peak at an inter atomic distance slightly larger than the blockade radius.

3 Random geometric graphs

Random geometric graphs (RGG) are a type of random graphs which can model the Rydberg blockade effect directly. The process of exciting particles until the jamming limit is reached is called random sequential adsorption (RSA) on a random graph. Random sequential adsorption is often associated with the parking problem, the problem of placing shapes in a volume at random until there is no space left to place a next shape. The problem is to derive how much of the volume is taken up by the shapes. The Rydberg blockade effect is an instance of such a parking problem. For dimensions higher than one, however, there are no analytical expressions known for the volume taken up by the shapes, or by the Rydberg spheres in our case. Therefore, other types of random graphs, on which random sequential adsorption is feasible analytically, are used as an approximation to RGG in later chapters. This chapter explores some of the properties which characterize random geometric graphs to be able to compare them later to different types of random graphs.

3.1 Properties of random geometric graphs

A formal definition of a random geometric graph is given below.

Definition: Random geometric graph
A random geometric graph $G = G(n, r, d)$ is defined by assigning each vertex $v \in \mathcal{V}(G)$ a position $x_v \in \mathbb{R}^d$ uniformly sampled from $[0, 1]^d$. Two vertices $v, w \in \mathcal{V}(G)$ are connected in the graph if their distance $\|x_v - x_w\|$ is less than or equal to r. The total number of vertices $|\mathcal{V}(G)|$ is equal to n.

Consider a vertex $v \in \mathcal{V}(G)$. The probability that another vertex $w \in \mathcal{V}(G)$ is connected to v is equal to the volume of a sphere with radius r. Moreover, because positions of the vertices are uniformly random, the event that a vertex w is connected to v is independent of each of the other connections to v. Hence, the number of neighbours of v is binomially distributed such that

$$\mathbb{P}(N_v = k) = \binom{n-1}{k} V_d(r)^k (1 - V_d(r))^{n-1-k}, \tag{3.1}$$

where N_v denotes the number of neighbours of v and $V_d(r)$ is the volume of a d-dimensional hypersphere given by

$$V_d(r) = \frac{\pi^{d/2} r^d}{\Gamma(d/2 + 1)}. \tag{3.2}$$

The mean number of neighbours c is equal to $(n-1)V_d(r)$. In a Rydberg gas the number of neighbours of an atom follows a Poisson distribution with parameter $\rho V_d(R_b)$ as argued in section 2.3. We now use a property of the binomial distribution to match the probability distributions of the number of neighbours in a random geometric graph and a Rydberg gas. Choosing $c = (n-1)V_d(r)$ constant and letting n go to infinity yields

$$\mathbb{P}(N_v = k) = \binom{n-1}{k} \left(\frac{c}{n-1}\right)^k \left(1 - \frac{c}{n-1}\right)^{n-1-k} \to \frac{c^k e^{-c}}{k!} \tag{3.3}$$

for the distribution of the number of neighbours in a random geometric graph. As can be seen, the binomial distribution converges to a Poisson distribution for $n \to \infty$. The random geometric graph is therefore related to the model of Rydberg atoms by setting $c = (n-1)V_d(r) = \rho V_d(R_b)$ constant and letting $n \to \infty$. The radius r should be decreased accordingly to keep c constant. The dimension d should be chosen as the dimension of space. Note that for $n \to \infty$ the random geometric graph can be fully described by the two parameters c and d.

	$\mathbf{E}[N_v]$	α	$\mathbb{P}(N_v = 0)$
RGG	c	$d\int_0^1 x^{d-1} I_{1-\frac{x^2}{4}}\left(\frac{d+1}{2}, \frac{1}{2}\right) dx$	e^{-c}

Table 1: Properties of a random geometric graph in the limit of $n \to \infty$. N_v denotes the number of neighbours of a vertex and α the clustering coefficient.

Another characteristic property is the clustering coefficient. The clustering coefficient α is defined by

$$\alpha = \mathbb{P}(v \leftrightarrow w \mid u \leftrightarrow v, u \leftrightarrow w). \tag{3.4}$$

The clustering coefficient therefore describes the probability of the third leg of a triangle appearing in the graph given that two of the legs of the triangle are present. In [12] it has been proven that the clustering coefficient converges to a constant independent of c for n tending to infinity. For $c > 0$ and $d \geq 1$,

$$\alpha \to d \int_0^1 x^{d-1} I_{1-\frac{x^2}{4}}\left(\frac{d+1}{2}, \frac{1}{2}\right) dx \tag{3.5}$$

as $n \to \infty$, where $I_z(a, b)$ is the normalized incomplete beta integral given by

$$I_z(a,b) = \frac{\int_0^z y^{a-1}(1-y)^{b-1} dy}{\int_0^1 y^{a-1}(1-y)^{b-1} dy}.$$

Finally, the probability of a vertex being isolated is

$$\mathbb{P}(N_v = 0) = (1 - V_d(r))^{n-1} = \left(1 - \frac{c}{n-1}\right)^{n-1} \to e^{-c} \tag{3.6}$$

where N_v again denotes the number of neighbours of a vertex v. For large c the probability of finding an isolated vertex becomes very small. As isolated, excited vertices block none of the other vertices, this property has a direct influence on the random sequential adsorption process. Table 1 summarizes the three properties discussed in this section.

3.2 Random sequential adsorption

Random sequential adsorption (RSA) on random graphs is the equivalent of exciting each of the atoms in a Rydberg gas until reaching the jamming limit. Consider a random graph G of which each vertex can be in either of three states: unaffected, activated or blocked. Initially all vertices are marked as unaffected. A single timestep of RSA consists of the following steps.

1. Select one of the unaffected vertices at random. Denote this vertex by v.
2. Mark v as activated.
3. Mark each of the neighbours of v as blocked.

This process continues until there are no unaffected vertices left in the graph at which point the jamming limit has been reached. For a random geometric graph this process is equivalent to exciting particles in a Rydberg gas because a vertex is only a neighbour of another vertex if these are distance r or less apart. Denote by X_∞ the number of activated particles in the jamming limit and recall that it is a random variable. The following theorems provide information about the convergence of X_∞ for n tending to infinity [13].

n	c	$\phi(c,2)$	$\sigma(c,2)$
400	0.3318	0.8592	0.08998
800	5.973	0.2538	0.03108
1600	11.95	0.1459	0.01326
2400	17.92	0.1030	0.008888
3200	23.90	0.07987	0.006516

Table 2: Scaled mean and variance of X_∞ after RSA using random geometric graphs in two dimensions (1000 simulations).

Theorem: LLN for RSA
Consider a random geometric graph $G = G(n, r, d)$. For all $c > 0$ and all $d \geq 1$ there exists a constant $\phi(c, d)$ such that

$$\frac{X_\infty}{n} \xrightarrow{\mathbb{P}} \phi(c, d) \tag{3.7}$$

as $n \to \infty$.

For a large graph, the fraction of the total number of vertices which needs to be activated to reach the jamming limit is likely to be close to $\phi(c, d)$. This also implies that the space taken up by the blockade spheres converges to a constant as $n \to \infty$.

Theorem: CLN for RSA
Consider a random geometric graph $G = G(n, r, d)$. For all $c > 0$ and all $d \geq 1$ there exists a constant $\sigma(c, d)$ such that

$$\frac{X_\infty - \mathbf{E}[X_\infty]}{\sqrt{n}} \xrightarrow{D} \mathcal{N}(0, \sigma(c, d)) \tag{3.8}$$

as $n \to \infty$, where $\mathcal{N}(\mu, \sigma)$ denotes a random variable with mean μ and variance σ.

These two powerful theorems tell us that there are constants which the mean and variance converge to without specifying the value for the constant itself. Numerical simulations have provided estimates for the limits of the two expressions [14] as well as analytical analysis using series expansions [15]. To our best knowledge, exact expressions of $\phi(c, d)$ and $\sigma(c, d)$ are known for one dimension only [16]. The limit of the mean is for instance given by

$$\phi(c, 1) = \frac{1}{c} \int_0^c \exp(-2 \int_0^v \frac{1 - e^{-x}}{x} dx) dv. \tag{3.9}$$

The expression for the variance is even more complicated and can be found in [16] for the interested. The complexity of equation (3.9) exemplifies the intricacy of doing analytical analysis on a random geometric graph. For $c \to \infty$ the expression reduces to $1/c$ times the Rényi constant [17]. Numerically this constant corresponds to 74.76%. In the jamming limit about three quarters of the space is therefore occupied by blockade spheres.

3.3 Performance

In the next chapters a model for random sequential adsorption on a random geometric graph is developed by substituting the random geometric graph by another random graph with similar properties. The results obtained from this model must be verified on their accuracy. Because there are no analytical expressions available, simulations will be used for comparison. Table 2 shows an excerpt of the results for the mean and variance after performing RSA on 1000 different instances of random geometric graphs for a varying mean number of neighbours. In total fifteen of these simulations will be used as benchmark to determine the accuracy of our models.

4 Erdős–Rényi graphs

One of the most basic types of random graphs are Erdős–Rényi graphs (ERG) [18]. In contrast to random geometric graphs, Erdős–Rényi graphs are random graphs without any form of spatial information. However, applying random sequential adsorption on Erdős–Rényi graphs is feasible analytically and yields expressions for the mean and variance of the number of activated particles. Depending on the degree of similarity between the two types of graphs, the resulting expressions can then serve as an estimate for $\phi(c, d)$ and $\sigma(c, d)$ for random geometric graphs. For one set of parameters, this type of random graphs has been used to estimate the expected value and variance with a relative error of 2.6% and 2.5% respectively [10]. This chapter details the process of random sequential adsorption on Erdős–Rényi graphs.

4.1 Properties of Erdős–Rényi graphs

The definition below introduces the Erdős–Rényi graph formally.

Definition: Erdős–Rényi graph
An Erdős–Rényi graph $G = G(n, p)$ is defined by connecting each vertex $v \in \mathcal{V}(G)$ to another vertex $w \in \mathcal{V}(G)$ with probability p independently of any of the other connections. The total number of vertices $|\mathcal{V}(G)|$ is equal to n.

Although the definition is simple compared to that of a random geometric graph, an Erdős–Rényi graph turns out to be a powerful predictor of the mean and variance of the number of activated particles. Consider a vertex $v \in \mathcal{V}(G)$. As each of the connections happens independently of the others with probability p, the number of neighbours of v is binomially distributed such that

$$\mathbb{P}(N_v = k) = \binom{n-1}{k} p^k (1-p)^{n-1-k}. \tag{4.1}$$

From comparing equations (3.3) and (4.1), it can be seen that p should be chosen as $c/(n-1)$. The distribution of the number of neighbours then becomes equal to that of a random geometric graph. Using a similar argument as before, the binomial distribution of the number of neighbours converges to a Poisson distribution with parameter c for $n \to \infty$. Therefore the distribution of the number of neighbours matches both the random geometric graph and the Rydberg gas. Note that for $n \to \infty$ the Erdős–Rényi graph is fully described by the single parameter c in contrast to the two parameters c and d for the random geometric graph.

Next, the clustering coefficient is investigated. For an Erdős–Rényi graph, the connections happen independently of each other. The clustering coefficient α thus reduces to

$$\alpha = \mathbb{P}(v \leftrightarrow w \mid u \leftrightarrow v, u \leftrightarrow w) = \mathbb{P}(v \leftrightarrow w) = p. \tag{4.2}$$

As $n \to \infty$ the clustering coefficient converges to zero because p has been chosen as $c/(n-1)$. This is a mismatch with the random geometric graph for which the clustering coefficient is strictly greater than zero for every choice of dimension d.

Finally, the probability of an isolated vertex occurring is

$$\mathbb{P}(N_v = 0) = (1-p)^{n-1} = \left(1 - \frac{c}{n-1}\right)^{n-1} \to e^{-c}. \tag{4.3}$$

The probability of finding an isolated vertex matches the random geometric graph exactly. This could also have been seen from the distribution of the number of neighbours of a vertex as this already matched the distribution of the number of neighbours in a random geometric graph. Substituting $k = 0$ in equation (4.1) is merely a specific case of this distribution. Table 3 summarizes the three properties discussed in this section in comparison to the properties of a random geometric graph.

	$\mathbf{E}[\,N_v]$	α	$\mathbb{P}(N_v = 0)$
RGG	c	$d\int_0^1 x^{d-1} I_{1-\frac{x^2}{4}}\left(\frac{d+1}{2}, \frac{1}{2}\right) dx$	e^{-c}
ERG	c	0	e^{-c}

Table 3: Properties of an Erdős–Rényi graph compared to a random geometric graph in the limit of $n \to \infty$. N_v denotes the number of neighbours of a vertex and α the clustering coefficient.

4.2 Random sequential adsorption

The random sequential adsorption process can be formalized for the Erdős–Rényi graph to obtain a Markov process. The idea is to track the number of unaffected vertices until this process has reached zero [10]. As on each timestep the number of activated vertices increases by one, the timestep at which the process hits zero gives the number of activated vertices in the jamming limit. Denote by U_t the number of unaffected vertices after t timesteps have passed. Initially $U_0 = n$. Now, at each timestep

$$U_t = U_{t-1} - 1 - \text{Bin}(U_{t-1} - 1, p). \tag{4.4}$$

In each timestep one vertex becomes activated and a binomial number of the remaining $U_{t-1} - 1$ vertices becomes blocked by the activated vertex. The random process is found to converge in probability to a deterministic function [19]. For $s \in [0, 1]$,

$$\frac{U_{\lfloor sn \rfloor}}{n} \xrightarrow{\mathbb{P}} u(s) \tag{4.5}$$

as $n \to \infty$, where $u(s) = e^{-cs} - (1 - e^{-cs})/c$. This means that in the limit of $n \to \infty$ the fraction of unaffected vertices behaves as a deterministic process. It is therefore possible to ascertain the time at which the process hits zero. At this point the jamming limit has been reached and the root s represents the fraction of activated vertices $\phi(c, d)$. Solving $u(s) = 0$ yields the following theorem, which can for example be found in [20].

Theorem: LLN for RSA
Consider an Erdős–Rényi graph $G = G(n, p)$. For all $c > 0$,

$$\frac{X_\infty}{n} \xrightarrow{\mathbb{P}} \frac{\ln(1 + c)}{c} \tag{4.6}$$

as $n \to \infty$.

To determine the variance, the process is scaled by $\sqrt{n}$. The scaled process converges to a normal variable in distribution,

$$\sqrt{n}\left(\frac{U_{\lfloor sn \rfloor}}{n} - u(s)\right) \xrightarrow{D} \mathcal{N}(0, v(s)), \tag{4.7}$$

as $n \to \infty$, where $v(s) = (1 - e^{-cs})((1 + 2c)e^{-cs} - 1)/(2c)$. Notice that $u'(\phi(c, d)) = -1$. The variance of X_∞ is therefore equal to the variance of $U_{\lfloor sn \rfloor}$ for $s = \phi(c, d)$ by applying the hitting time distribution theorem [21]. The next theorem is a direct result from [19].

Theorem: CLN for RSA
Consider an Erdős–Rényi graph $G = G(n, p)$. For all $c > 0$,

$$\frac{X_\infty - \mathbf{E}[\,X_\infty]}{\sqrt{n}} \xrightarrow{D} \mathcal{N}(0, \frac{c}{2(1 + c)^2}) \tag{4.8}$$

as $n \to \infty$.

It is important to realize that the two theorems above have exactly the same form as the theorems in the previous chapter about random geometric graphs. However, now expressions for the limits are known as we are considering Erdős–Rényi graphs.

4.3 Performance

The formulas have been compared to the test cases for random geometric graphs from the previous chapter. For each instance, the mean number of neighbours c has been matched with the simulation. In general both the mean and the variance are overestimated. The mean relative error is 25.4% for the mean and 83.6% for the variance.

The estimation is satisfactory for smaller values of c, while for larger values of c the estimation becomes worse. The best agreement is found for a value of $c = 0.6637$, which is the same value for c as used in the original article [10].

4.4 Mandel Q parameter

Until now the number of vertices n has been a discrete variable. In a Rydberg gas, however, the number of atoms N is a Poissonian random variable. The Mandel Q parameter can be easily calculated as

$$\begin{aligned} Q &= \frac{\mathrm{Var}(X_\infty)}{\mathbf{E}[\,X_\infty]} - 1 \\ &= \frac{\mathbf{E}[\,\mathrm{Var}(X_\infty \mid N)] + \mathrm{Var}(\mathbf{E}[\,X_\infty \mid N]\,)}{\mathbf{E}[\,\mathbf{E}[\,X_\infty \mid N]\,]} - 1 \\ &= \frac{\sigma(c,d)\mathbf{E}[\,N] + \phi(c,d)^2\mathrm{Var}(N)}{\phi(c,d)\mathbf{E}[\,N]} - 1 \\ &= \frac{\sigma(c,d)}{\phi(c,d)} + \phi(c,d) - 1, \end{aligned} \tag{4.9}$$

in general. The variables $\phi(c,d)$ and $\sigma(c,d)$ may be substituted with the proper expressions from this or the next chapters. The Mandel Q parameter will be estimated with an accuracy of the same order as the accuracy of the mean and the variance of the fraction of activated vertices. For the Erdős–Rényi graph, the error is even smaller because the mean and variance are both overestimated. As this explicit relationship between the Mandel Q parameter and the mean and variance of the number of activated vertices holds independently of the type of random graph used, the next chapters will focus solely on finding expressions for the latter two quantities and determining their accuracy.

5 Random intersection graphs

Random intersection graphs (RIG) are statistical network models, often committed to modeling social networks. Random intersection graphs are more sophisticated over Erdős–Rényi random graphs due to their ability to capture clustering effects [22]. In contrast, Erdős–Rényi graphs only allow for tuning the mean number of neighbours of a vertex. Random intersection graphs can therefore serve as a better substitute in the random sequential adsorption process.

5.1 Properties of random intersection graphs

The notation used is introduced in the formal definition below.

Definition: Binomial random intersection graph
A binomial random intersection graph $G = G(n, m, p)$ is defined by assigning each vertex $v \in \mathcal{V}(G)$ a set of attributes denoted by $\hat{A}_v \subseteq \mathcal{A}$. The probability of an attribute being assigned to a vertex is p, independently of other vertex-attribute connections. The total number of attributes $|\mathcal{A}|$ is equal to m. The number of attributes assigned to a vertex is thus binomially distributed, hence the name. The total number of vertices $|\mathcal{V}(G)|$ is equal to n. Two vertices $v, w \in \mathcal{V}(G)$ are connected whenever $\hat{A}_v \cap \hat{A}_w$ is nonempty, in other words whenever the vertices have at least one shared attribute.

A random intersection graph has a tendency to contain strongly connected communities, because each vertex connected to a certain attribute is connected to each other vertex connected to the same attribute. By choosing appropriate values for p and m, the expected number of neighbours of a vertex and the clustering coefficient can be adjusted.

To relate the random intersection graph to the other models for the Rydberg blockade effect, it is necessary to obtain expressions for the degree distribution and clustering coefficient. Consider a random intersection graph $G = G(n, m, p)$. In this graph the probability of two vertices $v, w \in \mathcal{V}(G)$ being connected is

$$\mathbb{P}(v \leftrightarrow w) = 1 - (1 - p^2)^m. \tag{5.1}$$

Hence, the expected number of neighbours N_v of a vertex is

$$\mathbf{E}[\, N_v] \, = (n-1)(1 - (1-p^2)^m) = (n-1)(mp^2 + O(m^2p^4)). \tag{5.2}$$

To obtain a non-trivial graph, the number of attributes should scale as a power of n [23]. The parameter m is thus set to $m = \lfloor \beta n^k \rfloor$ for some $k > 0$ and $\beta > 0$. To keep the expected degree constant as n tends to infinity, let $p = \gamma n^{-(1+k)/2}$ for some $\gamma > 0$. The expected degree then tends to $\beta\gamma^2$ as can be seen from equation (5.2).

The following two theorems have been proven in [24] and [25] respectively.

Theorem: Degree distribution
Consider the number of neighbours N_v of a vertex $v \in \mathcal{V}(G)$ in a random intersection graph $G(n, m, p)$ with parameters as defined above.

a) If $k < 1$, then N_v converges in distribution to a point mass at zero.

b) If $k = 1$, then N_v converges in distribution to a sum of a Poisson($\beta\gamma$) distributed number of Poisson(γ) variables, where all variables are independent.

c) If $k > 1$, then N_v is asymptotically Poisson($\beta\gamma^2$) distributed.

	$\mathbf{E}[N_v]$	α	$\mathbb{P}(N_v = 0)$
RGG	c	$d\int_0^1 x^{d-1} I_{1-\frac{x^2}{4}}\left(\frac{d+1}{2}, \frac{1}{2}\right) dx$	e^{-c}
ERG	c	0	e^{-c}
RIG	$\beta\gamma^2$	$(1+\beta\gamma)^{-1}$	$\exp(-\beta\gamma(1-e^{-\gamma}))$

Table 4: Properties of a random intersection graph compared to an Erdős–Rényi graph and a random geometric graph in the limit of $n \to \infty$. N_v denotes the number of neighbours of a vertex and α the clustering coefficient.

Theorem: Clustering coefficient
Consider the clustering coefficient α of a random intersection graph $G(n, m, p)$ with parameters as defined above.

a) If $k < 1$, then $\alpha \to 1$.

b) If $k = 1$, then $\alpha \to (1+\beta\gamma)^{-1}$.

c) If $k > 1$, then $\alpha \to 0$.

For a tunable clustering coefficient, it is therefore necessary to choose $k = 1$. The clustering coefficient is then equal to $(1+\beta\gamma)^{-1}$ for n tending to infinity. The number of neighbours of a vertex converges in distribution to a sum of a Poisson($\beta\gamma$) distributed number of Poisson(γ) variables. This is different from the distribution of the number of neighbours in a random geometric graph because in a random geometric graph, the number of neighbours follows a Poisson distribution. Nevertheless, the expected number of neighbours can be matched in both graphs. Note that in the limit of large n the random intersection graph can be fully described by the two parameters γ and β.

For a RIG the probability that a vertex is isolated is as follows.

$$\mathbb{P}(N_v = 0) = (1 - p + p(1-p)^{n-1})^m \to \exp(-\beta\gamma(1-e^{-\gamma})) \tag{5.3}$$

In general, this is not equal to the probability of finding an isolated vertex in the random geometric graph. This is also evident from the fact that the distributions of the number of neighbours are different. It can be seen, however, that for small values of γ the probability of finding an isolated vertex is matching with a random geometric graph.

$$\mathbb{P}(N_v = 0) = \exp(-\beta\gamma(1 - 1 + \gamma + O(\gamma^2))) = \exp(-\beta\gamma^2) + O(\beta\gamma^3) \tag{5.4}$$

Likewise, the number of neighbours is converging to a Poisson variable for γ tending to zero while keeping the mean number of neighbours constant. This can be seen from the theorem above. Note that the clustering coefficient is converging to zero in this case. In this limit, the Erdős–Rényi graph and the random intersection graph are therefore equal with respect to distribution of number of neighbours and degree of clustering. Also, a connection of two vertices becomes independent from other connections in this limit. The random intersection graph is therefore a direct generalization of the Erdős–Rényi graph [26]. Section 5.3 establishes that the resulting expression for random sequential adsorption matches the expression for an ERG as $\gamma \to 0$. Table 4 summarizes the three properties discussed in this section.

5.2 Random sequential adsorption

The process of random sequential adsorption on a random intersection graph is similar to RSA on an Erdős–Rényi graph. Instead of keeping track of only the number of unaffected particles U_t at each timestep, we should now also track the number of unaffected attributes W_t. Chapter 9 introduces the process formally and proves that the scaled processes converge to the following two deterministic functions.

$$\frac{U_{\lfloor sn \rfloor}}{n} \xrightarrow{\mathbb{P}} u(s), \qquad \frac{W_{\lfloor sn \rfloor}}{n} \xrightarrow{\mathbb{P}} w(s) \tag{5.5}$$

as $n \to \infty$, where

$$\begin{aligned} u(s) &= 1 - s - \int_0^s \gamma^2 u(x) w(x) dx, \\ w(s) &= \beta - \int_0^s \gamma w(x) dx. \end{aligned} \tag{5.6}$$

These functions have an intuitive interpretation. The process $w(s)$ starts out at β at timestep zero. In each next timestep the activated vertex blocks p times W_t attributes on average. The number of unaffected attributes decreases therefore by $\gamma w(s)$ in each timestep. The process $u(s)$ starts out at 1 at timestep zero. In each timestep there is one vertex which becomes activated. The number of unaffected vertices decreases thus by at least one. This vertex is connected to $\gamma w(s)$ attributes on average and each attribute is connected to $\gamma u(s)$ unaffected vertices in turn on average. The number of unaffected vertices therefore decreases by $1 + \gamma^2 u(s) w(s)$ in each timestep. Note that $w(s)$ can be further solved to $w(s) = \beta e^{-\gamma s}$.

The point at which $u(s)$ hits zero is the fraction of excited particles in the jamming limit as before. The following two theorems provide the mean and variance of the number of excited particles and are formally proved in chapter 9.

Theorem: LLN for RSA
Consider a random intersection graph $G = G(n, m, p)$. For all $\beta > 0$ and $\gamma > 0$,

$$\frac{X_\infty}{n} \xrightarrow{\mathbb{P}} \phi(\beta, \gamma) \tag{5.7}$$

as $n \to \infty$, where $\phi(\beta, \gamma)$ is the root of $u(s)$ as defined in equation (5.6).

Theorem: CLT for RSA
Consider a random intersection graph $G = G(n, m, p)$. For all $\beta > 0$ and $\gamma > 0$,

$$\frac{X_\infty - \mathbf{E}[X_\infty]}{\sqrt{n}} \xrightarrow{D} \mathcal{N}(0, \sigma_{uu}(\phi(\beta, \gamma))) \tag{5.8}$$

as $n \to \infty$, where

$$\begin{aligned} \sigma_{uu}(s) &= \exp(2\beta\gamma e^{-\gamma s}) \int_0^s \exp(-2\beta\gamma e^{-\gamma x}) \gamma^2 u(x)((1 + \gamma u(x)) w(x) - 2\sigma_{uw}(x)) dx, \\ \sigma_{uw}(s) &= \exp(\gamma(\beta e^{-\gamma s} - s)) \int_0^s \exp(-\gamma(\beta e^{-\gamma x} - x)) \gamma^2 u(x)(w(x) - \sigma_{ww}(x)) dx, \\ \sigma_{ww}(s) &= \exp(-2\gamma s) \int_0^s \exp(2\gamma x) \gamma w(x) dx = \beta e^{-\gamma s}(1 - e^{-\gamma s}). \end{aligned} \tag{5.9}$$

5.3 Correspondence with Erdős–Rényi

With the expressions obtained, it is interesting to determine the effects of the clustering coefficient on the fraction of activated vertices in the jamming limit. Recall that the clustering coefficient is given by $(1+\beta\gamma)^{-1}$ and the mean number of neighbours of a vertex by $\beta\gamma^2$. We choose a scaling parameter λ such that $\gamma \sim \lambda^{-1}$ and $\beta \sim \lambda^2$. When $\lambda \to \infty$, the clustering coefficient tends to zero. As γ becomes small, the following Taylor expansion can be used.

$$e^{-\gamma s} = 1 - \gamma s + O(\gamma^2) \tag{5.10}$$

Substituting the expression for $w(s)$ in equation (5.6) and solving the Volterra integral equation yields

$$u(s) = \exp(\beta\gamma e^{-\gamma s})(\exp(-\beta\gamma) - \int_0^s \exp(-\beta\gamma e^{-\gamma x})dx). \tag{5.11}$$

When using the Taylor expansion and neglecting the higher order terms, the expression can be further simplified to

$$\begin{aligned} u(s) &= \exp(\beta\gamma(1-\gamma s))(\exp(-\beta\gamma) - \int_0^s \exp(-\beta\gamma(1-\gamma x))dx) \\ &= \exp(-\beta\gamma^2 s)(1 - \int_0^s \exp(\beta\gamma^2 x)dx) \\ &= \exp(-\beta\gamma^2 s) - \frac{1-\exp(-\beta\gamma^2 s)}{\beta\gamma^2}, \end{aligned} \tag{5.12}$$

which is equivalent to the expression obtained for the Erdős–Rényi graph. A similar acquisition for the variance yields

$$\begin{aligned} \sigma_{uu}(s) &= \exp(-2\beta\gamma^2 s) \int_0^s \exp(2\beta\gamma^2 x)\gamma^2 u(x)(w(x) - 2\sigma_{uw}(x))dx \\ &= \exp(-2\beta\gamma^2 s) \int_0^s \exp(2\beta\gamma^2 x)\gamma^2(\exp(-\beta\gamma^2 x) - \frac{1-\exp(-\beta\gamma^2 x)}{\beta\gamma^2})\beta dx \\ &= \frac{(1-\exp(-\beta\gamma^2 s))((1+2\beta\gamma^2)\exp(-\beta\gamma^2 s) - 1)}{2\beta\gamma^2}, \end{aligned} \tag{5.13}$$

which is again equivalent to the expression obtained for the ERG. This shows that the random intersection graph with a small clustering coefficient yields the same result for the RSA process as the Erdős–Rényi graph.

When $\lambda \to 0$, the clustering coefficient tends to one. In this case equation (5.6) reduces to

$$\begin{aligned} u(s) &= \exp(\beta\gamma e^{-\gamma s})(\exp(-\beta\gamma) - \int_0^s \exp(-\beta\gamma e^{-\gamma x})dx) \\ &= 1 - s. \end{aligned} \tag{5.14}$$

Random sequential adsorption on a graph with a clustering coefficient of one seems to mean that each vertex should be activated before the jamming limit is reached. This implies a situation in which each vertex is isolated.

5.4 Performance

The formulas have been applied to the test cases of the random geometric graph. The parameters β and γ have been chosen to match the mean number of neighbours and the clustering coefficient of the random geometric graph as

$$\beta = \frac{(1-\alpha)^2}{\alpha^2 c}, \qquad \gamma = \frac{\alpha c}{1-\alpha}. \tag{5.15}$$

The mean relative errors are 139% and 913% for the mean and variance of the fraction of excited vertices respectively. The mean and variance are both severely overestimated by applying a random intersection graph. The estimation becomes worse for larger values of c.

It has been determined which value for the clustering coefficient yields the best estimate of the mean and variance while keeping the mean number of neighbours constant. For each choice of clustering coefficient the mean and variance are larger than the values obtained by the Erdős–Rényi graph. The mean and variance decrease by choosing a smaller clustering coefficient. As the Erdős–Rényi graph already overestimated these two quantities, the best agreement is found for a clustering coefficient tending to zero, for which the results from the Erdős–Rényi graph are obtained as discussed in the previous section.

Instead of matching the mean number of neighbours and the clustering coefficient with the random geometric graph, one could wonder what would happen if we match another combination of two properties. When trying to match the clustering coefficient and the probability of finding an isolated vertex, the latter probability becomes

$$\mathbb{P}(N_v = 0) = \exp(-\beta\gamma(1-e^{-\gamma})) > e^{-\beta\gamma}. \tag{5.16}$$

To see why this is problematic, consider a random geometric graph in two dimensions. For two dimensions, $\alpha \approx 0.587$ such that $\beta\gamma \approx 0.704$. For values of c larger than 0.704 the probability of finding an isolated vertex can thus never be matched with the probability of e^{-c} of finding an isolated vertex in a random geometric graph.

Finally, consider matching the mean number of neighbours and the probability of finding an isolated vertex. The latter probability is only equal to $e^{-\beta\gamma^2}$ for γ tending to zero. The distribution of the number of neighbours in that case converges to the distribution of the number of neighbours in a random geometric graph and the clustering coefficient converges to zero. In this limit the Erdős–Rényi graph is once again obtained.

6 Decomposed random intersection graphs

Although the random intersection graph is capable of matching both the mean number of neighbours and the clustering coefficient with a random geometric graph, its predictive capabilities when applied to random sequential adsorption are far worse than an Erdős–Rényi graph. Intuitively this is because of the differing distributions of the number of neighbours. In this chapter a novel type of random graph is introduced which is capable of matching the mean number of neighbours, the clustering coefficient and the probability of finding an isolated vertex with a random geometric graph. This model, the decomposed random intersection graph (DRIG), will turn out to be a significantly better predictor for the random sequential adsorption process.

6.1 Towards decomposed random intersection graphs

The definition of the decomposed random intersection graph, given in the next section, may seem quite complicated at first sight. This section aims at providing intuitive arguments which lead naturally to the definition of the decomposed random intersection graph. The DRIG is constructed by decomposing a random intersection graph in the subgraph consisting of vertices with at least one neighbour and the subgraph consisting of isolated vertices. To match the probability of finding an isolated vertex, vertices are either removed or added to the latter subgraph.

Consider a random intersection graph $G' = G'(n', \lfloor \beta n' \rfloor, \gamma/n')$. Denote the subgraph consisting of isolated vertices by $G'_0 \subseteq G'$ and the subgraph consisting of vertices with at least one neighbour by $G'_1 \subseteq G'$. The number of activated vertices X'_∞ in the random intersection graph can be decomposed as well as

$$X'_\infty = X'^0_\infty + X'^1_\infty, \tag{6.1}$$

where X'^0_∞ is the number of activated vertices in the subgraph G'_0 and X'^1_∞ is the number of activated vertices in the subgraph G'_1. Note that $X'^0_\infty = |G'_0|$ because an isolated vertex always becomes activated. Now, consider a decomposed random intersection graph $G = G(n, \beta, \gamma, c)$ constructed from this random intersection graph. Define the subgraphs $G_0 \subseteq G$ and $G_1 \subseteq G$ similarly as done for the random intersection graph. Recall that the probability of finding an isolated vertex in the random geometric graph is e^{-c}. Thus, to match the probability of finding an isolated vertex, we require

$$\frac{|G_0|}{n} \xrightarrow{\mathbb{P}} e^{-c} \quad \text{and} \quad \frac{|G_1|}{n} \xrightarrow{\mathbb{P}} 1 - e^{-c}, \tag{6.2}$$

as $n \to \infty$. This requirement constrains the size of both subgraphs in the limit of n tending to infinity. For the subgraph G_0 this requirement is enough to know the complete structure of G_0. The subgraph G_0 consists of only isolated vertices and knowing the number of vertices in the subgraph therefore determines the subgraph completely. For G_1, it is sensible to choose a graph which has the same mean number of neighbours, the same clustering coefficient and a zero probability of finding an isolated vertex. As the latter probability is indeed zero for G'_1 and the mean number of neighbours and the clustering coefficient can be tuned for a random intersection graph, we choose $G_1 = G'_1$. Chapter 9 proves that

$$\frac{|G'_1|}{n'} \xrightarrow{\mathbb{P}} 1 - y(\phi), \tag{6.3}$$

as $n' \to \infty$ where

$$y(s) = \exp(\beta\gamma e^{-\gamma}) \int_0^s \exp(-\beta\gamma e^{-\gamma x}) dx \tag{6.4}$$

and ϕ is the root of $u(s)$ as defined by equation (5.6).

To satisfy the requirement of equation (6.2), we must therefore choose

$$n' = \lfloor \frac{1-e^{-c}}{1-y(\phi)} n \rfloor. \tag{6.5}$$

This is enough to derive the law of large numbers for a decomposed random intersection graph.

To obtain the central limit theorem, it is necessary to define G_0 more elaborately. Denote the number of activated vertices in a decomposed random intersection graph by X_∞. This quantity can be written as the sum of X_∞^0 and X_∞^1 where X_∞^0 and X_∞^1 are the number of activated vertices in the subgraphs G_0 and G_1 respectively. Now,

$$\mathrm{Var}(\frac{X_\infty}{\sqrt{n}}) = \mathrm{Var}(\frac{X_\infty^1}{\sqrt{n}}) + \mathrm{Var}(\frac{X_\infty^0}{\sqrt{n}}) + 2\mathrm{Cov}(\frac{X_\infty^1}{\sqrt{n}}, \frac{X_\infty^0}{\sqrt{n}}). \tag{6.6}$$

Because G_1 has been chosen as G_1' before, the first term becomes

$$\mathrm{Var}(\frac{X_\infty^1}{\sqrt{n}}) = \frac{n'}{n}\mathrm{Var}(\frac{X_\infty'^1}{\sqrt{n'}}) = \frac{1-e^{-c}}{1-y(\phi)}\mathrm{Var}(\frac{X_\infty'^1}{\sqrt{n'}}), \tag{6.7}$$

for which an exact expression is known. Note that $X_\infty^0 = |G_0|$. With this observation, the second term can be calculated exactly from the random geometric graph and is equal to

$$\mathrm{Var}(\frac{X_\infty^0}{\sqrt{n}}) = e^{-c}(1-e^{-c}). \tag{6.8}$$

With a similar scaling argument as before, the third term can be estimated to be

$$\mathrm{Cov}(\frac{X_\infty^1}{\sqrt{n}}, \frac{X_\infty^0}{\sqrt{n}}) = \sqrt{\frac{e^{-c}(1-e^{-c})}{y(\phi)(1-y(\phi))}}\mathrm{Cov}(\frac{X_\infty'^1}{\sqrt{n'}}, \frac{X_\infty'^0}{\sqrt{n'}}). \tag{6.9}$$

This leads to two extra requirements on the quantity $|G_0| = X_\infty^0$. These two requirements are satisfied by the definition given in the next section.

6.2 Properties of decomposed random intersection graphs

In the following, denote by ϕ the root of $u(s)$ as defined by equation (5.6). The function $y(s)$ is defined by equation (6.4). Note that $y(\phi) = \exp(-\beta\gamma(1-e^{-\gamma}))$.

Definition: decomposed random intersection graph
Define n' by $n' = \lfloor \frac{1-e^{-c}}{1-y(\phi)} n \rfloor$. Construct a random intersection graph $G' = G'(n', \lfloor \beta n' \rfloor, \gamma/n')$ and decompose it into its subgraphs G_0' consisting of isolated vertices and G_1' consisting of vertices with at least one neighbour. The decomposed random intersection graph $G = G(n, \beta, \gamma, c)$ is defined as $G_0 \cup G_1'$ where G_0 is a graph consisting of merely isolated vertices and

$$|G_0| = \lfloor \sqrt{\frac{e^{-c}(1-y(\phi))}{y(\phi)(1-e^{-c})}}(|G_0'| - n'y(\phi)) + \mathcal{N}(ne^{-c}, n\sigma_0) \rfloor, \tag{6.10}$$

where

$$\sigma_0 = e^{-c}(1-e^{-c}) - \frac{e^{-c}}{y(\phi)}\mathrm{Var}(\frac{|G_0'|}{\sqrt{n'}}). \tag{6.11}$$

We now examine the properties of the decomposed random intersection graph. Either adding or removing isolated vertices to a graph does not change the clustering coefficient of the graph in any way. The clustering coefficient of a graph is thus fully determined by the subgraph consisting of vertices with at least one neighbour. For the DRIG, the clustering coefficient is therefore still $(1+\beta\gamma)^{-1}$ as $n \to \infty$, which is equal to the clustering coefficient of a random intersection graph.

	$\mathbf{E}[\,N_v]$	α	$\mathbb{P}(N_v = 0)$
RGG	c	$d\int_0^1 x^{d-1} I_{1-\frac{x^2}{4}}\left(\frac{d+1}{2}, \frac{1}{2}\right) dx$	e^{-c}
ERG	c	0	e^{-c}
RIG	$\beta\gamma^2$	$(1+\beta\gamma)^{-1}$	$\exp(-\beta\gamma(1-e^{-\gamma}))$
DRIG	$(1-e^{-c})\frac{\beta\gamma^2}{1-\exp(-\beta\gamma(1-e^{-\gamma}))}$	$(1+\beta\gamma)^{-1}$	e^{-c}

Table 5: Properties of DRIG compared to the other types of random graphs in the limit of $n \to \infty$. N_v denotes the number of neighbours of a vertex and α the clustering coefficient.

Using equation (6.3), the size of subgraph G_0 is found to converge in probability as

$$\frac{|G_0|}{n} \xrightarrow{\mathbb{P}} e^{-c}, \tag{6.12}$$

for $n \to \infty$. Likewise, the number of vertices in the subgraph G_1' converges in probability as

$$\frac{|G_1'|}{n} = \frac{n'}{n}\frac{|G_1'|}{n'} \xrightarrow{\mathbb{P}} \frac{1-e^{-c}}{1-y(\phi)}(1-y(\phi)) = 1-e^{-c}. \tag{6.13}$$

Therefore, as $n \to \infty$, the probability that a vertex $v \in \mathcal{V}(G)$ is isolated is

$$\mathbb{P}(N_v = 0) = \mathbb{P}(v \in G_0) = \frac{e^{-c}}{e^{-c} + (1-e^{-c})} = e^{-c}. \tag{6.14}$$

Finally, the mean number of neighbours of a vertex $v \in \mathcal{V}(G)$ is

$$\mathbf{E}[\,N_v] \,= \mathbb{P}(N_v > 0)\mathbf{E}[\,N_v \mid N_v > 0] \,= (1-e^{-c})\frac{\beta\gamma^2}{1-y(\phi)}. \tag{6.15}$$

Table 5 summarizes the three properties.

6.3 Random sequential adsorption

The following theorem establishes the convergence of the number of activated vertices in the DRIG.

Theorem: LLN for RSA
Consider a decomposed random intersection graph $G = G(n, \beta, \gamma, c)$. For all $\beta > 0$, $\gamma > 0$ and $c > 0$,

$$\frac{X_\infty}{n} \xrightarrow{\mathbb{P}} e^{-c} + (1-e^{-c})\frac{\phi(\beta,\gamma) - \exp(-\beta\gamma(1-e^{-\gamma}))}{1-\exp(-\beta\gamma(1-e^{-\gamma}))} \tag{6.16}$$

where $\phi(\beta, \gamma)$ is the root of $u(s)$ as defined in equation (5.6).

Proof. Denote by X_∞^0 the number of activated vertices in the jamming limit in the subgraph G_0 and by $X_\infty^{'1}$ the number of activated vertices in the subgraph G_1'. Notice that $X_\infty^0 = |G_0|$ as an isolated vertex always becomes activated. Then,

$$\frac{X_\infty}{n} = \frac{X_\infty^0}{n} + \frac{X_\infty^{'1}}{n} = \frac{|G_0|}{n} + \frac{n'}{n}\frac{X_\infty^{'1}}{n'}. \tag{6.17}$$

Each of the terms in equation (6.17) converges in probability. Denoting the total number of activated vertices in the random intersection graph by X_∞', the last term converges to

$$\frac{X_\infty^{'1}}{n'} = \frac{X_\infty'}{n'} - \frac{|G_0'|}{n'} \xrightarrow{\mathbb{P}} \phi(\beta,\gamma) - y(\phi) \tag{6.18}$$

by the law of large numbers for a random intersection graph and the convergence of the number of isolated vertices.

Therefore,

$$\frac{X_\infty}{n} \xrightarrow{\mathbb{P}} e^{-c} + (1-e^{-c})\frac{\phi(\beta,\gamma) - \exp(-\beta\gamma(1-e^{-\gamma}))}{1-\exp(-\beta\gamma(1-e^{-\gamma}))}, \tag{6.19}$$

which proves the theorem.

■

Theorem: CLT for RSA
Consider a decomposed random intersection graph $G = G(n,\beta,\gamma,c)$. For all $\beta > 0$, $\gamma > 0$ and $c > 0$,

$$\frac{X_\infty - \mathbf{E}[X_\infty]}{\sqrt{n}} \xrightarrow{D} \mathcal{N}(0, \sigma_{xx}(\beta,\gamma,c)) \tag{6.20}$$

as $n \to \infty$, where

$$\begin{aligned}\sigma_{xx}(\beta,\gamma,c) = {} & \frac{1-e^{-c}}{1-y(\phi)}((1-y'(\phi))^2\sigma_{uu}(\phi) - 2(1-y'(\phi))\sigma_{uy}(\phi) + \sigma_{yy}(\phi)) \\ & + 2\sqrt{\frac{e^{-c}(1-e^{-c})}{y(\phi)(1-y(\phi))}}(y'(\phi)(1-y'(\phi))\sigma_{uu}(\phi) + (1-2y'(\phi))\sigma_{uy}(\phi) - \sigma_{yy}(\phi)) \\ & + e^{-c}(1-e^{-c})\end{aligned} \tag{6.21}$$

and

$$\begin{aligned}\sigma_{uu}(s) &= \exp(2\beta\gamma e^{-\gamma s})\int_0^s \exp(-2\beta\gamma e^{-\gamma x})\gamma^2 u(x)((1+\gamma u(x))w(x) - 2\sigma_{uw}(x))dx, \\ \sigma_{uw}(s) &= \exp(\gamma(\beta e^{-\gamma s} - s))\int_0^s \exp(-\gamma(\beta e^{-\gamma x} - x))\gamma^2 u(x)(w(x) - \sigma_{ww}(x))dx, \\ \sigma_{ww}(s) &= \exp(-2\gamma s)\int_0^s \exp(2\gamma x)\gamma w(x)dx = \beta e^{-\gamma s}(1-e^{-\gamma s}), \\ \sigma_{wy}(s) &= \exp(-\gamma s)\int_0^s \exp(\gamma x)\gamma(1-e^{-\gamma(1-x)})g(x,w(x))(w(x) - \sigma_{ww}(x))dx, \\ \sigma_{uy}(s) &= \exp(\beta\gamma e^{-\gamma s})\int_0^s \exp(-\beta\gamma e^{-\gamma x})(-\gamma(1-e^{-\gamma(1-x)})g(x,w(x))\sigma_{uw}(x) \\ &\quad + \gamma^2 u(x)(w(x)g(x,w(x)) - \sigma_{wy}(x)))dx, \\ \sigma_{yy}(s) &= \int_0^s -2\gamma(1-e^{-\gamma(1-x)})g(x,w(x))\sigma_{wy}(x) + g(x,w(x))(1-g(x,w(x)))dx.\end{aligned} \tag{6.22}$$

Proof. Consider X^1_∞ and X^0_∞ as defined previously. For X^1_∞,

$$\frac{X^1_\infty - \mathbf{E}[\,X^1_\infty]}{\sqrt{n}} = \sqrt{\frac{n'}{n}}\frac{X'^1_\infty - \mathbf{E}[\,X'^1_\infty]}{\sqrt{n'}} = \sqrt{\frac{1-e^{-c}}{1-y(\phi)}}\left(\frac{X'_\infty - \mathbf{E}[\,X'_\infty]}{\sqrt{n'}} - \frac{X'^0_\infty - \mathbf{E}[\,X'^0_\infty]}{\sqrt{n'}}\right). \tag{6.23}$$

Now, the theorem in the previous chapter has shown that

$$\frac{X'_\infty - \mathbf{E}[\,X'_\infty]}{\sqrt{n'}} \xrightarrow{D} U(\phi), \tag{6.24}$$

and by the proof of chapter 9,

$$\frac{X'^0_\infty - \mathbf{E}[\,X'^0_\infty]}{\sqrt{n'}} = \frac{|G'_0| - \mathbf{E}[\,|G'_0|]}{\sqrt{n'}} \xrightarrow{D} Y(\phi) + U(\phi)y'(\phi), \tag{6.25}$$

where $U(s)$ and $Y(s)$ are normal random variables with mean zero and covariance matrix

$$\begin{pmatrix}\sigma_{uu}(s) & \sigma_{uy}(s)\\ \sigma_{uy}(s) & \sigma_{yy}(s)\end{pmatrix}. \tag{6.26}$$

For X^0_∞,

$$\frac{X^0_\infty - \mathbf{E}[\,X^0_\infty]}{\sqrt{n}} = \frac{|G_0| - \mathbf{E}[\,|G_0|]}{\sqrt{n}} \xrightarrow{D} \sqrt{\frac{e^{-c}}{y(\phi)}}(Y(\phi) + U(\phi)y'(\phi)) + \mathcal{N}(0,\sigma_0). \tag{6.27}$$

Noting that the sum of a set of normal random variables is also a normal variable and combining the variance and covariance terms proves the theorem.

■

6.4 Performance

The formulas resulting from the previous two theorems have been applied to the test cases of the random geometric graph. The mean relative error for the mean number of activated vertices is 3.0%. The estimation again becomes worse for increasing values of c. However, the adapted model predicts the mean more than eight times more accurate than an Erdős–Rényi graph in terms of relative error. For $c = 0.6637$, the relative error is 0.4%. Figure 5 displays the relative error for the different types of graphs. The decomposed random intersection graph underestimates the mean number of activated vertices in general.

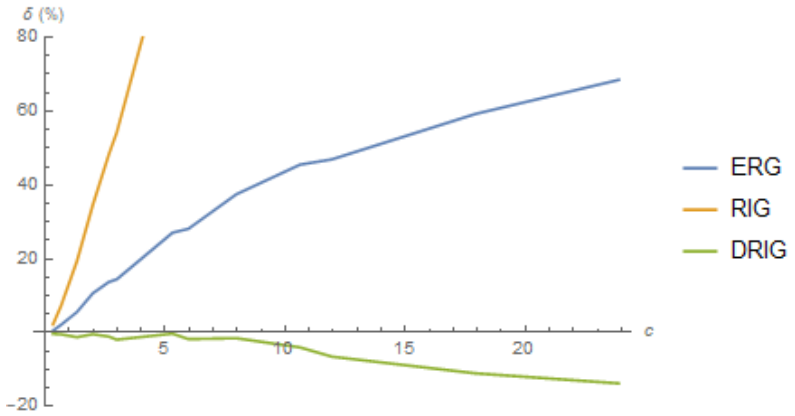

Figure 5: The relative error (δ) of the mean number of activated vertices for different values of c.

The mean relative error for the variance of the number of activated vertices is 33.2% over all test cases. The improvement with respect to Erdős–Rényi graphs is most apparent for larger values of c. For these values of c the relative error is close to 33%, slightly overestimating the variance. The improvement over the Erdős–Rényi is about six times for these values. For smaller values of c, the Erdős–Rényi graph performs better. Figure 6 shows the relative error for different values of c, comparing the different types of graphs. For $c < 2$, the decomposed random intersection graph underestimates instead of overestimates the variance.

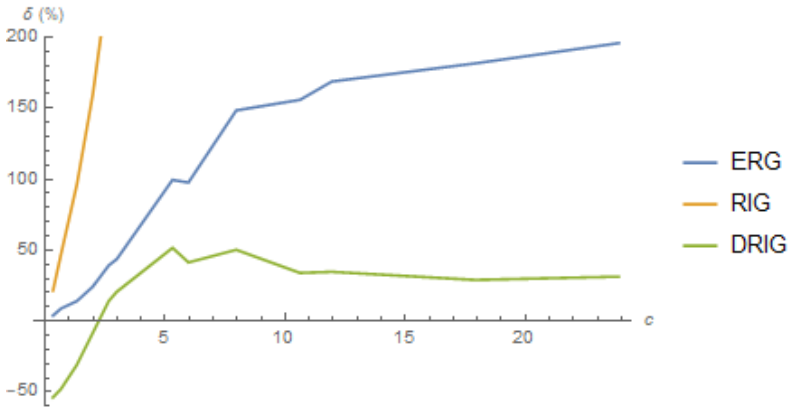

Figure 6: The relative error (δ) in the variance of the number of activated vertices for different values of c.

7 Pair correlation

One disadvantage of using random graphs for describing the Rydberg blockade effect is the loss of spatial information. In both the random intersection graph and the Erdős–Rényi graph a notion such as the position of a vertex does not exist. In the Rydberg blockade experiment, one often measures the pair correlation $g(R)$. The pair correlation is defined as the normalized probability of two vertices being excited given that they are a distance R apart. However, due to the absence of spatial information, the distance between vertices is not directly observable in a random intersection graph. This chapter explores the possibilities for using other metrics on a random graph and relating these metrics to the distance between vertices to obtain a measure for the pair correlation.

Recall the definition of the pair correlation presented earlier in equation (2.3). Note that this expression is only observable in a random geometric graph.

7.1 Graph distance

A metric for distance used on random graphs is the graph distance. The graph distance $d_G(v, w)$ between two vertices $v, w \in \mathcal{V}(G)$ is defined as the minimum number of edges one needs to pass when moving from v to w in the graph. A graph distance of one means that the vertices are directly connected. It then becomes possible to relate the pair correlation to the graph distance.

$$\begin{aligned} &\mathbb{P}(v, w \in \hat{X}_\infty \mid d(v, w) \in [R, R+\delta)) = \\ &\sum_{i=0}^{\infty} \mathbb{P}(v, w \in \hat{X}_\infty \mid d_G(v, w) = i) \mathbb{P}(d_G(v, w) = i \mid d(v, w) \in [R, R+\delta)), \end{aligned} \tag{7.1}$$

where $\hat{X}_\infty$ denotes the set of activated vertices in the jamming limit as before. Note that conditional independence has been used between the probability of the two vertices being excited and their distance, given their graph distance, as

$$\mathbb{P}(v, w \in \hat{X}_\infty \mid d_G(v, w) = i, d(v, w) \in [R, R+\delta)) \approx \mathbb{P}(v, w \in \hat{X}_\infty \mid d_G(v, w) = i). \tag{7.2}$$

The assumption here is that the graph distance gives enough of the spatial information originally present in the Euclidean distance to leave out this condition. This is not a trivial assumption and it will be checked whether this assumption is reasonable.

The first term in the sum is independent of the Euclidean distance between two vertices and can thus be observed in a random graph such as the random intersection graph. The second term is depending on the Euclidean distance between vertices. However, the second term is independent of the RSA process. In the literature, expressions for the last term in the sum have been looked into closely. Although an analytical expression is not known at this point to our best knowledge, upper and lower bounds on the graph distance have been found [27].

Figure 7a displays the actual pair correlation measured on simulations of random geometric graphs. Figure 7b then shows the estimated pair correlation by using equation 7.1. Both terms have been simulated on random geometric graphs as to check whether the assumption of conditional independence is reasonable. Apart from the peak around the blockade radius, the agreement between the two graphs is striking.

The shape of the pair correlation, especially the height of the first peak, strongly depends on the chosen value for c. For smaller values of c the peak generally becomes smaller. When the Rydberg blockade effect is small, that is for small values of the blockade radius, spatial correlations are less present. This explains the less apparent peak for smaller c. The larger the value for c, the denser the packing becomes and the more spatial correlations occur. The approximation using graph distances quite closely resembles the pair correlation, although for increasing values of c the estimation becomes worse. Also, the peak at a distance slightly larger than the blockade radius is usually estimated smaller and has not been found to become larger than 1.2.

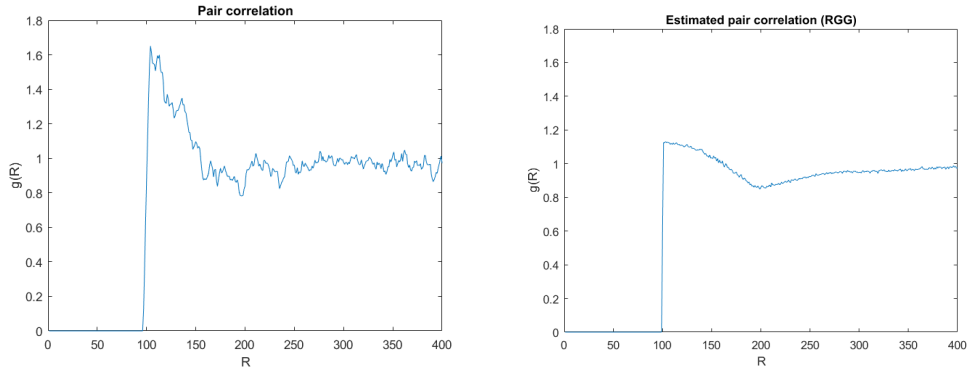

(a) (b)

Figure 7: Figure (a) shows the pair correlation by simulating 5000 instances of random geometric graphs with $n = 200$ and $c = 6.28$. Figure (b) shows the pair correlation by using the graph distance. Both graphs use a blockade radius of 100.

Next, we substitute the first term in the sum by a term simulated from a random intersection graph. Figure 8a displays the result. Figure 8b shows the result when using an Erdős–Rényi graph instead. The results are quite different from the graphs seen in Figure 7. This implies that the graph structures are too different to yield useful results for the pair correlation. Using a decomposed random intersection graph instead of the regular random intersection graph did not change the results significantly. The decomposed random intersection graph has the same probabilities for having vertices at a certain graph distance. Adding or removing the number of isolated vertices merely changes the probability at a graph distance of infinity.

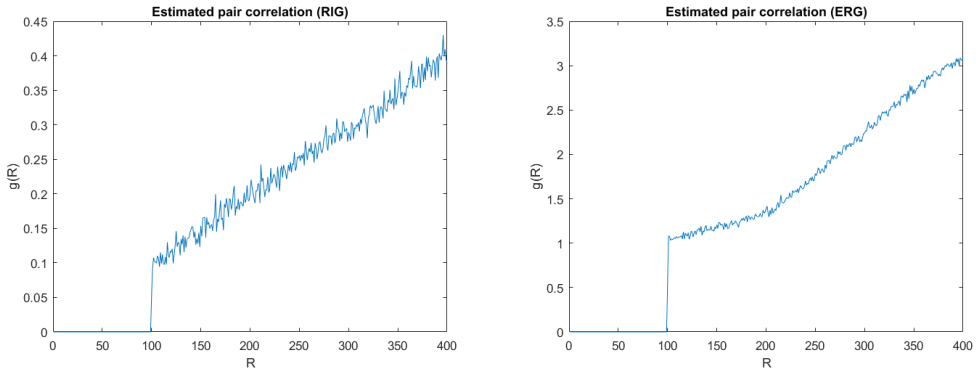

(a) (b)

Figure 8: Figure (a) shows the pair correlation by using the graph distance of simulations of 5000 instances of random intersection graphs with $n = 200$ and $c = 6.28$. Figure (b) shows the pair correlation by using the graph distance with Erdős–Rényi graphs.

Figure 9 displays the first term in the sum of equation (7.1) for different types of random graphs. The disagreement between the different types of random graphs explains the deviant estimation of the pair correlation. Note that the results in Figure 9 are far from trivial and interesting in their own right. Explaining or describing these results quantitatively has not been pursued in this thesis and is left for future research.

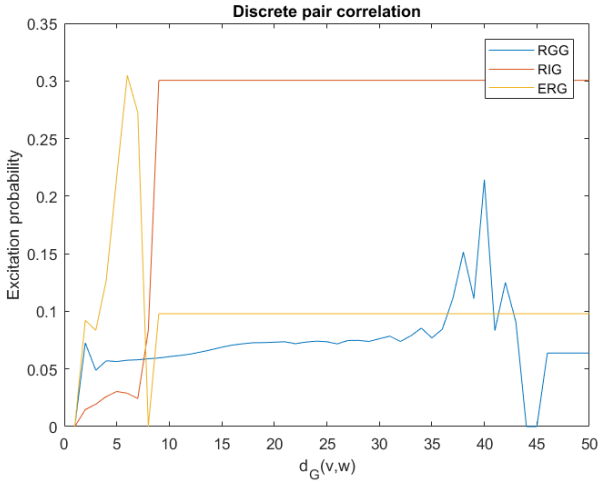

Figure 9: The probability of finding two excited particles at a certain graph distance using simulations of 1000 instances of different random graphs with $n = 200$ and $c = 6.28$.

Another drawback of using this method, except for the disagreement seen in Figures 7a and 7b, is the following. The goal of substituting a different type of random graph instead of the random geometric graph is the attempt of obtaining an analytical expression for the pair correlation. As discussed before, the random sequential adsorption process on random geometric graphs is difficult to analyze analytically. Even if the estimation for the pair correlation would be acceptable when using a random intersection graph instead of a random geometric graph, an analytical expression for the pair correlation is still not directly obtainable. The problem is the second term in the sum for which no analytical expression is known. Searching for an analytical expression for the first term in the sum therefore seems fruitless at this point.

7.2 Common neighbours

Another metric for distance between two vertices in a random graph is the number of neighbours two vertices have in common. Intuitively, the more neighbours the vertices have in common the smaller the distance between the two. This argument is formalized as

$$\mathbb{P}(v, w \in \hat{X}_\infty \mid d(v,w) \in [R, R+\delta)) =$$
$$\sum_{i=0}^{\infty} \mathbb{P}(v, w \in \hat{X}_\infty \mid N_w = i, d(v,w) \in [R, R+\delta)) \mathbb{P}(N_w = i \mid d(v,w) \in [R, R+\delta)) =$$
$$\sum_{i=0}^{\infty} \sum_{j=0}^{\infty} \mathbb{P}(v, w \in \hat{X}_\infty \mid |\hat{N}_v \cap \hat{N}_w| = j, N_w = i) \mathbb{P}(|\hat{N}_v \cap \hat{N}_w| = j \mid N_w = i, d(v,w) \in [R, R+\delta)) \mathbb{P}(N_w = i). \tag{7.3}$$

This time the assumption has been made of conditional independence between two vertices being excited and their Euclidean distance, given the number of shared neighbours between the two.

$$\mathbb{P}(v, w \in \hat{X}_\infty \mid |\hat{N}_v \cap \hat{N}_w| = j, N_w = i, d(v,w) \in [R, R+\delta)) \approx \mathbb{P}(v, w \in \hat{X}_\infty \mid |\hat{N}_v \cap \hat{N}_w| = j, N_w = i) \tag{7.4}$$

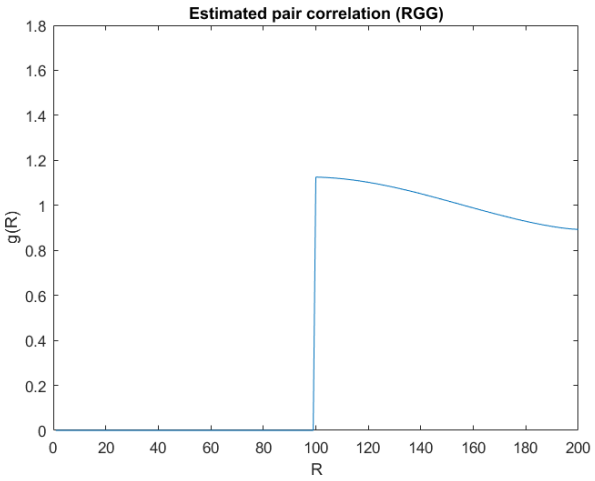

Figure 10: The pair correlation by using the number of common neighbours of simulations of 5000 instances of random geometric graphs with $n = 200$ and $c = 6.28$. The graph uses a blockade radius of 100.

Figure 10 shows the estimated pair correlation by simulating the first term in the sum on random geometric graphs. The graph shows similar agreement to the pair correlation as when using graph distance as a metric. Figure 11a and 11b show the pair correlation when using random intersection graphs and Erdős–Rényi graphs respectively. Note the similarities between using an Erdős–Rényi graph and a random geometric graph in this case. The Erdős–Rényi graph seems an appropriate predictor for the pair correlation which has been observed for a wide range of values of c. Even for larger values of c the Erdős–Rényi graph seems to approximate the pair correlation well, the peak around the blockade radius growing as expected.

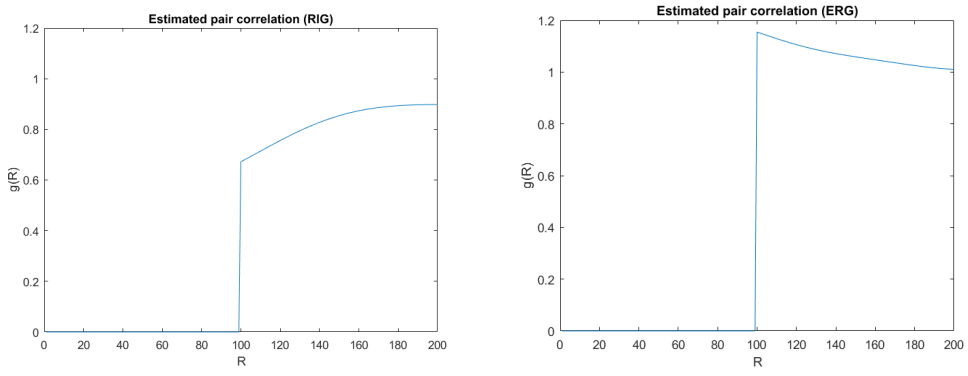

(a) (b)

Figure 11: Figure (a) shows the pair correlation by using the number of common neighbours of simulations of 5000 instances of random intersection graphs with $n = 200$ and $c = 6.28$. Figure (b) shows the pair correlation by using the number of common neighbours in Erdős–Rényi graphs.

Figure 12 shows the first term in the sum of equation (7.3) for different values of N_w. The shape of the graphs is remarkably similar for different values of N_w. The probability therefore seems to depend only on the *fraction* of common neighbours. This observation could be used as an additional assumption to achieve an even better estimate of the pair correlation and is left to future research.

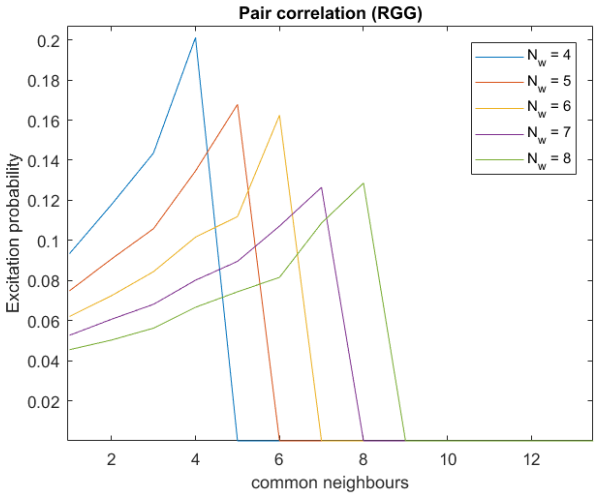

Figure 12: The probability of finding two excited vertices depending on their number of common neighbours by using simulations of 5000 instances of random geometric graphs with $n = 200$ and $c = 6.28$.

The advantage of using the number of common neighbours over the graph distance is the prospect of finding an analytical expression for the pair correlation. The first term in the sum of equation (7.3) can be found analytically by adapting the random sequential adsorption process. The second term can be found by noting that

$$|\hat{N}_v \cap \hat{N}_w| \stackrel{d}{=} \mathrm{Bin}(i, p) \tag{7.5}$$

where p is given by

$$p = \mathbb{P}(u \in \hat{N}_v \mid u \in \hat{N}_w, d(v, w) \in [R, R + \delta)). \tag{7.6}$$

Previously the Rydberg blockade effect was modeled with hard spheres. When a particle is in the sphere, it has a probability of zero of becoming excited while outside the sphere the particle experiences no influence from the excitation. When using hard spheres, p is the volume shared by the spheres when the vertices are a distance R apart divided by the volume of a single sphere $V_d(R_b)$. This restricts the use of this method to a maximum distance of $2R_b$. For distances larger than $2R_b$ the above probability becomes zero. However, if the assumption of hard spheres is dropped, the usable distance can be arbitrarily extended. Denote the distance from u to the line through v and w by $u_\perp$ and denote the position of u relative to w projected on the line from w to v by $u_\parallel$. If δ is taken to zero, the probability p is then given by

$$\begin{aligned}
p &= \int_0^\infty \int_{-\infty}^\infty \mathbb{P}(u \in \hat{N}_v, u_\perp = s, u_\parallel = t \mid u \in \hat{N}_w, d(v, w) = R) dt ds \\
&= \int_0^\infty \int_{-\infty}^\infty \mathbb{P}(u \in \hat{N}_v \mid u_\perp = s, u_\parallel = t) \mathbb{P}(u_\perp = s, u_\parallel = t \mid u \in \hat{N}_w) dt ds \\
&= \frac{\int_0^\infty \int_{-\infty}^\infty \mathbb{P}(u \in \hat{N}_v \mid d(v, u) = \sqrt{s^2 + (R - t)^2}) \mathbb{P}(u \in \hat{N}_w \mid d(w, u) = \sqrt{s^2 + t^2}) dt ds}{\int_0^\infty \int_{-\infty}^\infty \mathbb{P}(u \in \hat{N}_w \mid d(w, u) = \sqrt{s^2 + t^2}) dt ds}.
\end{aligned} \tag{7.7}$$

Notice that if

$$\mathbb{P}(u \in \hat{N}_w \mid d(w,u) = R) = \begin{cases} 0, & \text{if } R \leq R_b \\ 1, & \text{if } R > R_b \end{cases}, \tag{7.8}$$

as is the case for hard spheres, the probability p indeed reduces to the volume shared by the spheres divided by the volume of a single sphere $V_d(R_b)$.

The final term in the sum of equation (7.3) is simply determined by the probability distribution of the number of neighbours.

$$\mathbb{P}(N_w = i) = \frac{c^i e^{-c}}{i!} \tag{7.9}$$

Using this method, an analytical expression for the pair correlation can thus be found. Extending the random sequential adsorption process to calculate the first term in the sum analytically is left for future research.

8 Conclusion

In this thesis an extensive overview of describing the Rydberg blockade effect by random graphs has been given. The random geometric graph has been introduced which is capable of describing the Rydberg blockade effect exactly. Analytical analysis on random geometric graphs has been difficult and expressions for the random sequential adsorption process are only known for one dimension. Therefore random graphs such as the Erdős–Rényi graph have been analyzed previously in the literature. The Erdős–Rényi graph has been compared to the random geometric graph by three properties: the mean number of neighbours, the clustering coefficient and the probability of a vertex being isolated. The Erdős–Rényi graph matches two of the properties, while the clustering coefficient is zero for an Erdős–Rényi compared to a value strictly larger than zero for the random geometric graph. Nonetheless the ERG forms a wonderful predictor of the random sequential adsorption process by achieving a mean relative error of 25.4% and 83.6% for the mean and variance of the number of activated vertices respectively.

Next, random sequential adsorption has been applied to the random intersection graph. Proofs of the law of large numbers and the central limit theorem for RSA have been given. The random intersection graph turned out to be a direct generalization for the Erdős–Rényi graph. By matching the mean number of neighbours and the clustering coefficient, the random intersection graph performed a mean relative error of 139% and 913% for the mean and variance respectively. In general, the random intersection graph severely overestimated both the mean and variance. The best correspondence to the random geometric graph has been found by matching the mean number of neighbours and the probability of a vertex being isolated in which case the random intersection graph reduces to an Erdős–Rényi graph.

In an attempt to increase the accuracy for a random intersection graph, a novel type of random graph, the decomposed random intersection graph, has been introduced. The decomposed random intersection graph is capable of matching each of the three properties with a random geometric graph. The probability of a vertex being isolated is matched by either adding or removing isolated vertices to a random intersection graph. The DRIG achieves a mean relative error of 3.0% and 33.2% on the mean and variance respectively. It therefore is a better predictor than the Erdős–Rényi graph in terms of relative error.

Finally, a method of measuring the pair correlation on random graphs has been set forward. While a random graph in general possesses no notion of position, two metrics observable on a random graph have been used to obtain a measure for the pair correlation. In terms of graph distance, both a random intersection graph and an Erdős–Rényi graph behave too differently to yield useful results for the pair correlation. Moreover, the method of using graph distances offers no prospect of finding an analytical expression for the pair correlation in the near future. On the other hand, using the number of common neighbours of two vertices as a metric for distance is fruitful for an Erdős–Rényi graph. Furthermore, by measuring the number of common neighbours on an Erdős–Rényi graph even an analytical expression for the pair correlation can be found.

The research in this thesis contributes to a better understanding of the behaviour of the Rydberg blockade effect. The more accurate prediction of the Mandel Q parameter can serve practical purposes in experiments. The topic of pair correlation, although explored only shallowly, is promising and deserves future scientific interest.

9 Proof: RSA on a random intersection graph

In random sequential adsorption on a graph, one sequentially selects a vertex in a graph and marks the vertex as activated. The direct neighbours of the activated vertex are marked as blocked. Blocked vertices are restricted from becoming activated and vertices are activated only once. Vertices cannot be deactivated once activated. This process continues until all vertices are either activated or blocked, a state labeled as the jamming limit. This chapter establishes the proof for the law of large numbers and the central limit theorem for the number of activated vertices in a random intersection graph in the jamming limit as introduced in section 5.2.

The idea is to track both the number of unaffected vertices and the number of unaffected attributes. While not strictly necessary for a random intersection graph, the number of activated, isolated vertices is also kept track of. The expressions involving the number of isolated vertices are merely used for the adapted model in chapter 6. The scaled processes can be decomposed in a drift part, which converges to a deterministic function, and a martingale part. The martingale part vanishes as n tends to infinity when scaled by n. When scaled by $\sqrt{n}$, the martingale part produces a system of differential equations for the variance. The approach taken is similar to [12].

9.1 State description

During the random sequential adsorption process, four quantities will be kept track of. These quantities are given by the following definitions.

Define $\hat{X}_t \subseteq \mathcal{V}(G)$ as the set of all activated vertices at timestep t. For brevity, denote $|\hat{X}_t|$ as X_t.

Define $\hat{U}_t \subseteq \mathcal{V}(G)$ as the set of all unaffected vertices at timestep t. Unaffected vertices are vertices which are neither blocked nor activated. Denote $|\hat{U}_t|$ as U_t.

Define $\hat{W}_t \subseteq \mathcal{A}$ as the set of all unaffected attributes at timestep t. Unaffected attributes are attributes for which none of the connected vertices are activated. Denote $|\hat{W}_t|$ as W_t.

Define $\hat{Y}_t \subseteq \mathcal{V}(G)$ as the set of all isolated, activated vertices at timestep t. Denote $|\hat{Y}_t|$ as Y_t.

The random sequential adsorption process can be characterized in terms of these four sets. Although Y_t is formally not necessary for representing random sequential adsorption, it will be used in the decomposed random intersection graph. At timestep zero,

$$\begin{aligned} \hat{X}_0 &= \varnothing, \\ \hat{U}_0 &= \mathcal{V}(G), \\ \hat{W}_0 &= \mathcal{A}, \\ \hat{Y}_0 &= \varnothing. \end{aligned} \tag{9.1}$$

At each next timestep t, a vertex $v \in \hat{U}_{t-1}$ becomes activated whenever $\hat{U}_{t-1}$ is nonempty. When $\hat{U}_{t-1}$ is empty, the jamming limit has been reached and the number of activated vertices is X_{t-1}. Define $\hat{N}_v$ by $\hat{N}_v = \{w \in \mathcal{V}(G) \mid \hat{A}_v \cap \hat{A}_w \neq \varnothing, v \neq w\}$ or in other words the neighbours of the activated vertex. Then,

$$\begin{aligned} \hat{X}_t &= \hat{X}_{t-1} \cup \{v\}, \\ \hat{U}_t &= \hat{U}_{t-1} \setminus (\{v\} \cup \hat{N}_v), \\ \hat{W}_t &= \hat{W}_{t-1} \setminus \hat{A}_v, \\ \hat{Y}_t &= \begin{cases} \hat{Y}_{t-1} \cup \{v\}, & \text{if } \hat{N}_v = \varnothing \\ \hat{Y}_{t-1}, & \text{otherwise} \end{cases}. \end{aligned} \tag{9.2}$$

It suffices to look at the size of each set. If $\hat{U}_t$ is empty then U_t is zero and the jamming limit has been reached. Note that $X_t = t$ such that the number of activated vertices in the jamming limit is simply t (if the process ends at timestep t). For the binomial random intersection graph the number of attributes of a vertex is binomially distributed. Denote the number of connected attributes $|\hat{A}_v|$ by A_v. Conditional on W_{t-1}, the number of connected attributes of the activated vertex is

$$A_v \overset{d}{=} \mathrm{Bin}(W_{t-1}, p). \tag{9.3}$$

Note that $v \in \hat{U}_{t-1}$ and it is therefore restricted from having connections with activated attributes. The number of connected attributes must thus be binomial with the number of unaffected attributes and probability p. Now,

$$\begin{aligned} U_t &= U_{t-1} - dU_t, \\ W_t &= W_{t-1} - dW_t, \\ Y_t &= Y_{t-1} + dY_t, \end{aligned} \tag{9.4}$$

where

$$\begin{aligned} dU_t &\overset{d}{=} 1 + \mathrm{Bin}(U_{t-1} - 1, 1 - (1-p)^{A_v}), \\ dW_t &= A_v, \\ dY_t &\overset{d}{=} \mathrm{Ber}((1-p)^{A_v(n-t)}). \end{aligned} \tag{9.5}$$

Therefore (U_t, W_t, Y_t) is a Markov process. Notice that (U_t, W_t) by itself is also a Markov process. The expectation of dU_t conditional on the previous timestep is

$$\begin{aligned} \mathbf{E}[\, dU_t \mid U_{t-1}, W_{t-1}, Y_{t-1}] &= 1 + (U_{t-1} - 1)(1 - \mathbf{E}[\, (1-p)^{A_v} \mid U_{t-1}, W_{t-1}]\,) \\ &= 1 + (U_{t-1} - 1)(1 - (1 - p + p(1-p))^{W_{t-1}}) \\ &= 1 + (U_{t-1} - 1)(1 - (1-p^2)^{W_{t-1}}). \end{aligned} \tag{9.6}$$

For dW_t the conditional expectation is given by

$$\mathbf{E}[\, dW_t \mid U_{t-1}, W_{t-1}, Y_{t-1}] = pW_{t-1}. \tag{9.7}$$

Finally, the conditional expectation of dY_t is given by

$$\mathbf{E}[\, dY_t \mid U_{t-1}, W_{t-1}, Y_{t-1}] = (1 - p + p(1-p)^{n-t})^{W_{t-1}}. \tag{9.8}$$

9.2 Martingale decomposition

Using the Doob-Meyer decomposition [28] of U_t yields the following martingale decomposition

$$U_t = n - \sum_{i=1}^{t} dU_t = n + M_n^u(t) - t - \sum_{i=1}^{t} (U_{i-1} - 1)(1 - (1-p^2)^{W_{i-1}}), \tag{9.9}$$

where $M_n^u(t)$ is a square-integrable martingale. Using a Taylor expansion, the term in the sum is asymptotically equal to

$$1 - (1-p^2)^{W_{i-1}} = 1 - (1 - p^2 W_{i-1} + O_{\mathbb{P}}(p^4 W_{i-1}^2)) = \frac{\gamma^2 W_{i-1}}{n^2} + O_{\mathbb{P}}(n^{-2}). \tag{9.10}$$

Define the scaled processes

$$u_n(s) = \frac{U_{\lfloor sn \rfloor}}{n}, \quad w_n(s) = \frac{W_{\lfloor sn \rfloor}}{n} \quad \text{and} \quad y_n(s) = \frac{Y_{\lfloor sn \rfloor}}{n}. \tag{9.11}$$

Then, the scaled process $u_n(s)$ in is given by

$$\begin{aligned} u_n(s) &= 1 + \frac{M_n^u(\lfloor sn \rfloor)}{n} - \frac{\lfloor sn \rfloor}{n} - \frac{1}{n}\sum_{i=1}^{\lfloor sn \rfloor} \frac{U_{i-1}}{n}\frac{\gamma^2 W_{i-1}}{n} + O_{\mathbb{P}}(n^{-1}) \\ &= 1 + \frac{M_n^u(\lfloor sn \rfloor)}{n} - s - \int_0^s \gamma^2 u_n(x) w_n(x) dx + O_{\mathbb{P}}(n^{-1}). \end{aligned} \tag{9.12}$$

A similar acquisition for W_t yields

$$W_t = m - \sum_{i=1}^{t} dW_t = m + M_n^w(t) - \sum_{i=1}^{t} pW_{i-1}, \tag{9.13}$$

where $M_n^w(t)$ is again a square-integrable martingale. The scaled process is given by

$$\begin{aligned} w_n(s) &= \frac{m}{n} + \frac{M_n^w(\lfloor sn \rfloor)}{n} - \frac{1}{n}\sum_{i=1}^{\lfloor sn \rfloor} pW_{t-1} \\ &= \beta + \frac{M_n^w(\lfloor sn \rfloor)}{n} - \int_0^s \gamma w_n(x) dx. \end{aligned} \tag{9.14}$$

Finally, the Doob-Meyer decomposition of Y_t yields the following martingale decomposition

$$Y_t = \sum_{i=1}^{t} dY_t = M_n^y(t) + \sum_{i=1}^{t} (1 - p + p(1-p)^{n-i})^{W_{i-1}}, \tag{9.15}$$

where $M_n^y(t)$ is a square-integrable martingale. The scaled process is given by

$$\begin{aligned} y_n(s) &= \frac{M_n^y(\lfloor sn \rfloor)}{n} + \frac{1}{n}\sum_{i=1}^{\lfloor sn \rfloor} (1 - p + p(1-p)^{n-i})^{W_{i-1}} \\ &= \frac{M_n^y(\lfloor sn \rfloor)}{n} + \int_0^s \exp(-\gamma w_n(x)(1 - e^{-\gamma(1-x)})) dx. \end{aligned} \tag{9.16}$$

9.3 Quadratic variation and covariation

To prove the convergence of $u_n(s)$, $w_n(s)$ and $y_n(s)$, the quadratic variation and covariation terms of the martingales $M_n^u(t)$, $M_n^w(t)$ and $M_n^y(t)$ are needed. Denote the variance conditional on (U_t, W_t, Y_t) as Var_t, the covariance similarly as Cov_t and the expected value as $\mathbf{E}_t$. The quadratic variation and covariation are given by

$$\begin{aligned}
\langle M_n^u \rangle(t) &= \sum_{i=1}^{t} \mathrm{Var}_{i-1}(dU_i), \\
\langle M_n^w \rangle(t) &= \sum_{i=1}^{t} \mathrm{Var}_{i-1}(dW_i), \\
\langle M_n^y \rangle(t) &= \sum_{i=1}^{t} \mathrm{Var}_{i-1}(dY_i), \\
\langle M_n^u, M_n^w \rangle(t) &= \sum_{i=1}^{t} \mathrm{Cov}_{i-1}(dU_i, dW_i), \\
\langle M_n^w, M_n^y \rangle(t) &= \sum_{i=1}^{t} -\mathrm{Cov}_{i-1}(dW_i, dY_i), \\
\langle M_n^u, M_n^y \rangle(t) &= \sum_{i=1}^{t} -\mathrm{Cov}_{i-1}(dU_i, dY_i).
\end{aligned} \tag{9.17}$$

The minus sign in the last two expressions appears due to the sign in the definition in equation (9.4). We start with the term for the quadratic variation of $M_n^u(t)$. Using the law of total variance,

$$\mathrm{Var}_{t-1}(dU_t) = \mathbf{E}_{t-1}[\,\mathrm{Var}_{t-1}(dU_t \mid A_v)] + \mathrm{Var}_{t-1}(\mathbf{E}_{t-1}[\,dU_t \mid A_v]\,). \tag{9.18}$$

The first term expands to

$$\begin{aligned}
\mathbf{E}_{t-1}[\,\mathrm{Var}_{t-1}(dU_t \mid A_v)] &= (U_{t-1}-1)\mathbf{E}_{t-1}[\,(1-p)^{A_v}(1-(1-p)^{A_v})] \\
&= (U_{t-1}-1)(\mathbf{E}_{t-1}[\,(1-p)^{A_v}] - \mathbf{E}_{t-1}[\,(1-p)^{2A_v}]\,) \\
&= (U_{t-1}-1)((1-p+p(1-p))^{W_{t-1}} - (1-p+p(1-p)^2)^{W_{t-1}}) \\
&= (U_{t-1}-1)((1-p^2)^{W_{t-1}} - (1-2p^2+p^3)^{W_{t-1}}),
\end{aligned} \tag{9.19}$$

and the second term to

$$\begin{aligned}
\mathrm{Var}_{t-1}(\mathbf{E}_{t-1}[\,dU_t \mid A_v]\,) &= (U_{t-1}-1)^2\mathrm{Var}_{t-1}((1-p)^{A_v}) \\
&= (U_{t-1}-1)^2(\mathbf{E}_{t-1}[\,(1-p)^{2A_v}] - \mathbf{E}[\,(1-p)^{A_v}]^{\,2}) \\
&= (U_{t-1}-1)^2((1-2p^2+p^3)^{W_{t-1}} - (1-p^2)^{2W_{t-1}}) \\
&= (U_{t-1}-1)^2((1-2p^2+p^3)^{W_{t-1}} - (1-2p^2+p^4)^{W_{t-1}}).
\end{aligned} \tag{9.20}$$

The two terms can be combined to form the quadratic variation of $M_n^u(t)$. The term in the quadratic variation of $M_n^w(t)$ is simply

$$\mathrm{Var}_{t-1}(dW_t) = p(1-p)W_{t-1}. \tag{9.21}$$

The term in the quadratic variation of $M_n^y(t)$ is

$$\mathrm{Var}_{t-1}(dY_t) = \mathbf{E}_{t-1}[\,dY_t]\,(1 - \mathbf{E}_{t-1}[\,dY_t]\,). \tag{9.22}$$

Finally, we determine the terms necessary for the covariation. The covariation of dU_i and dW_i is defined as

$$\mathrm{Cov}_{t-1}(dU_t, dW_t) = \mathbf{E}_{t-1}[\,dU_t dW_t] \,-\, \mathbf{E}_{t-1}[\,dU_t]\,\mathbf{E}_{t-1}[\,dW_t]\,. \tag{9.23}$$

The first term is equal to

$$\begin{aligned}
\mathbf{E}_{t-1}[\,dU_t dW_t] &= \mathbf{E}_{t-1}[\,\mathbf{E}_{t-1}[\,dU_t dW_t \mid A_v]\,] \\
&= \mathbf{E}_{t-1}[\,A_v(1 + (U_{t-1} - 1)(1 - (1-p)^{A_v}))] \\
&= \mathbf{E}_{t-1}[\,A_v(1 + (U_{t-1} - 1))] \,-\, (U_{t-1} - 1)\mathbf{E}_{t-1}[\,A_v(1-p)^{A_v}] \\
&= pW_{t-1}U_{t-1} - (U_{t-1} - 1)pW_{t-1}(1-p)(1 - p + p(1-p))^{W_{t-1}-1} \\
&= pW_{t-1}(U_{t-1} - (U_{t-1} - 1)(1-p)(1-p^2)^{W_{t-1}-1}),
\end{aligned} \tag{9.24}$$

and the second term is

$$\begin{aligned}
\mathbf{E}_{t-1}[\,dU_t]\,\mathbf{E}_{t-1}[\,dW_t] &= pW_{t-1}(1 + (U_{t-1} - 1)(1 - (1-p^2)^{W_{t-1}})) \\
&= pW_{t-1}(U_{t-1} - (U_{t-1} - 1)(1-p^2)^{W_{t-1}})).
\end{aligned} \tag{9.25}$$

Therefore,

$$\mathrm{Cov}_{t-1}(dU_t, dW_t) = pW_{t-1}(U_{t-1} - 1)(p - p^2)(1-p^2)^{W_{t-1}-1}. \tag{9.26}$$

The quadratic covariation of $M_n^w(t)$ and $M_n^y(t)$ is derived as

$$\begin{aligned}
\mathbf{E}_{t-1}[\,dW_t dY_t] &= \mathbf{E}_{t-1}[\,\mathbf{E}_{t-1}[\,dW_t dY_t \mid A_v]\,] \\
&= \mathbf{E}_{t-1}[\,A_v(1-p)^{A_v(n-t)}] \\
&= \frac{pW_{t-1}(1 - p + p(1-p)^{n-t})^{W_{t-1}}(1-p)^n}{p(1-p)^n + (1-p)(1-p)^t},
\end{aligned} \tag{9.27}$$

resulting in

$$\mathrm{Cov}_{t-1}(dW_t, dY_t) = -pW_{t-1}(1 - p + p(1-p)^{n-t})^{W_{t-1}} \left(1 - \frac{(1-p)^n}{p(1-p)^n + (1-p)(1-p)^t}\right). \tag{9.28}$$

Finally,

$$\mathbf{E}_{t-1}[\,dU_t dY_t] \,=\, \mathbf{E}_{t-1}[\,\mathbf{E}_{t-1}[\,dU_t dY_t \mid dY_t]\,] \,=\, \mathbf{E}_{t-1}[\,dY_t]\,. \tag{9.29}$$

The covariance of dU_t and dY_t is thus

$$\begin{aligned}
\mathrm{Cov}_{t-1}(dU_t, dY_t) &= (1 - p + p(1-p)^{n-t})^{W_{t-1}}(1 - (1 + (U_{t-1} - 1)(1 - (1-p^2)^{W_{t-1}}))) \\
&= -(1 - p + p(1-p)^{n-t})^{W_{t-1}}(U_{t-1} - 1)(1 - (1-p^2)^{W_{t-1}}).
\end{aligned} \tag{9.30}$$

Based on the quadratic variation terms above, the following lemma holds.

Lemma: Convergence of martingales
As $n \to \infty$,

$$\frac{1}{n}\sup_{s\in[0,1]}|M_n^u(\lfloor sn\rfloor)| \xrightarrow{\mathbb{P}} 0, \qquad \frac{1}{n}\sup_{s\in[0,1]}|M_n^w(\lfloor sn\rfloor)| \xrightarrow{\mathbb{P}} 0, \qquad \frac{1}{n}\sup_{s\in[0,1]}|M_n^y(\lfloor sn\rfloor)| \xrightarrow{\mathbb{P}} 0 \tag{9.31}$$

Proof. Observe the following.

$$\begin{aligned}(1-p^2)^{W_{t-1}} &= 1 + O_{\mathbb{P}}(n^{-1}),\\ (1-2p^2+p^3)^{W_{t-1}} &= 1 + O_{\mathbb{P}}(n^{-1}),\\ (1-2p^2+p^3)^{W_{t-1}} &= (1-2p^2)^{W_{t-1}} + O_{\mathbb{P}}(n^{-2}),\\ (1-2p^2+p^4)^{W_{t-1}} &= (1-2p^2)^{W_{t-1}} + O_{\mathbb{P}}(n^{-3}).\end{aligned} \tag{9.32}$$

Therefore $\mathrm{Var}_{t-1}(dU_t) = O_{\mathbb{P}}(1)$. Moreover, also $\mathrm{Var}_{t-1}(dW_t) = O_{\mathbb{P}}(1)$ and $\mathrm{Var}_{t-1}(dY_t) = O_{\mathbb{P}}(1)$. Thus from equation (9.17), for any $s \in [0,1]$,

$$\langle M_n^u\rangle(\lfloor sn\rfloor) = O_{\mathbb{P}}(n), \qquad \langle M_n^w\rangle(\lfloor sn\rfloor) = O_{\mathbb{P}}(n), \qquad \langle M_n^y\rangle(\lfloor sn\rfloor) = O_{\mathbb{P}}(n). \tag{9.33}$$

Then the proof follows from Doob's inequality [29].

■

9.4 Convergence of the scaled processes

Define the limits of the scaled processes as

$$\begin{aligned}u(s) &= 1 - s - \int_0^s \gamma^2 u(x)w(x)dx,\\ w(s) &= \beta - \int_0^s \gamma w(x)dx,\\ y(s) &= \int_0^s \exp(-\gamma w(x)(1-e^{-\gamma(1-x)}))dx.\end{aligned} \tag{9.34}$$

For notational convenience, denote by $g(x,w)$ the function $g(x,w) = \exp(-\gamma w(1-e^{-\gamma(1-x)}))$. We show that the scaled processes converge to the above limits. Starting with $w_n(s)$,

$$\begin{aligned}\sup_{s\in[0,1]}|w_n(s) - w(s)| &\le \sup_{s\in[0,1]}\frac{|M_n^w(\lfloor ns\rfloor)|}{n} + \gamma\int_0^1 \sup_{s\in[0,x]}|w_n(s)-w(s)|dx\\ &\le \sup_{s\in[0,1]}\frac{|M_n^w(\lfloor ns\rfloor)|}{n}e^{\gamma} \xrightarrow{\mathbb{P}} 0,\end{aligned} \tag{9.35}$$

using Grönwall's inequality [21] and the previous lemma. Notice that the function $f(u,w) = uw$ is Lipschitz continuous on $[0,1]\times[0,\beta]$. Therefore there exists a constant $C_1 > 0$ such that for all $s \in [0,1]$,

$$|u_n(s)w_n(s) - u(s)w(s)| \le C_1(|u_n(s)-u(s)| + |w_n(s)-w(s)|). \tag{9.36}$$

Thus,

$$\begin{aligned}\sup_{s\in[0,1]}|u_n(s)-u(s)| &\le \sup_{s\in[0,1]}\frac{|M_n^u(\lfloor ns\rfloor)|}{n}+\gamma^2\int_0^1\sup_{s\in[0,x]}|u_n(s)w_n(s)-u(s)w(s)|dx\\ &\le \sup_{s\in[0,1]}\frac{|M_n^w(\lfloor ns\rfloor)|}{n}+\gamma^2C_1\sup_{s\in[0,1]}|w_n(s)-w(s)|+\gamma^2C_1\int_0^1\sup_{s\in[0,x]}|u_n(s)-u(s)|dx\\ &\le \left(\sup_{s\in[0,1]}\frac{|M_n^w(\lfloor ns\rfloor)|}{n}+\gamma^2C_1\sup_{s\in[0,1]}|w_n(s)-w(s)|\right)e^{\gamma^2C_1}\xrightarrow{\mathbb{P}}0,\end{aligned} \tag{9.37}$$

again using Grönwall's inequality and the previous lemma. The function $g(x,w)=\exp(-\gamma w(1-e^{-\gamma(1-x)}))$ as defined above is Lipschitz continuous as a function of w on $[0,\beta]$. Therefore there exists a constant $C_2>0$ such that for all $s\in[0,1]$,

$$|g(s,w_n(s))-g(s,w(s))|\le C_2|w_n(s)-w(s)|. \tag{9.38}$$

Thus,

$$\begin{aligned}\sup_{s\in[0,1]}|y_n(s)-y(s)| &\le \sup_{s\in[0,1]}\frac{|M_n^y(\lfloor ns\rfloor)|}{n}+\int_0^1\sup_{s\in[0,x]}|g(s,w_n(s))-g(s,w(s))|dx\\ &\le \sup_{s\in[0,1]}\frac{|M_n^y(\lfloor ns\rfloor)|}{n}+C_2\sup_{s\in[0,1]}|w_n(s)-w(s)|\xrightarrow{\mathbb{P}}0\end{aligned} \tag{9.39}$$

This proves that the scaled processes converge to their limits as defined by (9.34). Note that the root of $u(s)$ is always smaller than one. The root of $u(s)$ must therefore give the fraction of activated vertices in the jamming limit, which proves the law of large numbers for a random intersection graph.

■

Equation (9.34) can be further solved to give the following.

$$\begin{aligned}u(s)&=\exp(\beta\gamma e^{-\gamma s})(\exp(-\beta\gamma)-\int_0^s\exp(-\beta\gamma e^{-\gamma x})dx),\\ w(s)&=\beta e^{-\gamma s},\\ y(s)&=\exp(\beta\gamma e^{-\gamma})\int_0^s\exp(-\beta\gamma e^{-\gamma x})dx\end{aligned} \tag{9.40}$$

Note that $y(\phi)=\exp(-\beta\gamma(1-e^{-\gamma}))$ where ϕ is the root of $u(s)$.

9.5 Diffusion scaled processes

Define the diffusion scaled processes

$$\bar{U}_n(s) = \sqrt{n}(u_n(s) - u(s)), \quad \bar{W}_n(s) = \sqrt{n}(w_n(s) - w(s)), \quad \bar{Y}_n(s) = \sqrt{n}(y_n(s) - y(s)) \tag{9.41}$$

and the diffusion scaled martingales

$$\bar{M}_n^u(t) = \frac{M_n^u(\lfloor ns \rfloor)}{\sqrt{n}}, \qquad \bar{M}_n^w(t) = \frac{M_n^w(\lfloor ns \rfloor)}{\sqrt{n}}, \qquad \bar{M}_n^y(t) = \frac{M_n^y(\lfloor ns \rfloor)}{\sqrt{n}}. \tag{9.42}$$

Rewriting the diffusion scaled processes yields

$$\begin{aligned} \bar{U}_n(s) &= \bar{M}_n^u(t) - \gamma^2\sqrt{n}\int_0^s u_n(x)w_n(x) - u(x)w(x)dx + O_{\mathbb{P}}(n^{-\frac{1}{2}}) \\ &= \bar{M}_n^u(t) - \int_0^s \gamma^2 w_n(x)\bar{U}_n(x)dx - \int_0^s \gamma^2 u(x)\bar{W}_n(x)dx + O_{\mathbb{P}}(n^{-\frac{1}{2}}) \end{aligned} \tag{9.43}$$

and

$$\begin{aligned} \bar{W}_n(s) &= \bar{M}_n^w(t) - \gamma\sqrt{n}\int_0^s w_n(x) - w(x)dx \\ &= \bar{M}_n^w(t) - \int_0^s \gamma\bar{W}_n(x)dx \end{aligned} \tag{9.44}$$

and

$$\bar{Y}_n(s) = \bar{M}_n^y(t) + \sqrt{n}\int_0^s \exp(-\gamma w_n(x)(1 - e^{-\gamma(1-x)})) - \exp(-\gamma w(x)(1 - e^{-\gamma(1-x)}))dx. \tag{9.45}$$

Using a Taylor expansion of $g(x, w) = \exp(-\gamma w(1 - e^{-\gamma(1-x)}))$ with respect to w yields

$$g(x, w_n(x)) = g(x, w(x)) - \gamma(1 - e^{-\gamma(1-x)})g(x, w(x))(w_n(x) - w(x)) + O_{\mathbb{P}}((w_n(x) - w(x))^2). \tag{9.46}$$

Now, notice that $n^{1/4}(w_n(x) - w(x)) \xrightarrow{\mathbb{P}} 0$ by the proof of the lemma showing the convergence of martingales and following the steps in the previous section. Therefore,

$$\bar{Y}_n(s) = \bar{M}_n^y(t) - \int_0^s \gamma(1 - e^{-\gamma(1-x)})g(x, w(x))\bar{W}_n(x)dx + o_{\mathbb{P}}(1). \tag{9.47}$$

The quadratic variation and covariation of the martingales can be used to show that the scaled martingales converge to a diffusion process. The quadratic variation of $\bar{M}_n^u$ is given by

$$\begin{aligned} \langle \bar{M}_n^u \rangle(s) &= \frac{1}{n}\sum_{i=1}^{\lfloor sn \rfloor} \mathrm{Var}_{i-1}(dU_i) \\ &= \frac{1}{n}\sum_{i=1}^{\lfloor sn \rfloor} U_{t-1}(p^2 W_{t-1} + O_{\mathbb{P}}(n^{-2})) + U_{t-1}^2(p^3 W_{t-1} + O_{\mathbb{P}}(n^{-3})) \\ &\xrightarrow{\mathbb{P}} \int_0^s \gamma^2 u(x)w(x) + \gamma^3 u(x)^2 w(x)dx. \end{aligned} \tag{9.48}$$

For $\bar{M}_n^w$,

$$\begin{aligned}\langle \bar{M}_n^w \rangle(s) &= \frac{1}{n}\sum_{i=1}^{\lfloor sn \rfloor} \mathrm{Var}_{i-1}(dW_i) \\ &= \frac{1}{n}\sum_{i=1}^{\lfloor sn \rfloor} p(1-p)W_{t-1} \xrightarrow{\mathbb{P}} \int_0^s \gamma w(x)dx\end{aligned} \tag{9.49}$$

For $\bar{M}_n^y$,

$$\begin{aligned}\langle \bar{M}_n^y \rangle(s) &= \frac{1}{n}\sum_{i=1}^{\lfloor sn \rfloor} \mathrm{Var}_{i-1}(dY_i) \\ &= \frac{1}{n}\sum_{i=1}^{\lfloor sn \rfloor} (1-p+p(1-p)^{n-t})^{W_{i-1}}(1-(1-p+p(1-p)^{n-t})^{W_{i-1}}) \\ &\xrightarrow{\mathbb{P}} \int_0^s g(x,w(x))(1-g(x,w(x)))dx\end{aligned} \tag{9.50}$$

The quadratic covariation of $\bar{M}_n^u$ and $\bar{M}_n^w$ is

$$\begin{aligned}\langle \bar{M}_n^u, \bar{M}_n^w \rangle(s) &= \frac{1}{n}\sum_{i=1}^{\lfloor sn \rfloor} \mathrm{Cov}_{i-1}(dU_i, dW_i) \\ &= \frac{1}{n}\sum_{i=1}^{\lfloor sn \rfloor} p^2 U_{t-1}W_{t-1} + O_{\mathbb{P}}(n^{-1}) \\ &\xrightarrow{\mathbb{P}} \int_0^s \gamma^2 u(x)w(x)dx.\end{aligned} \tag{9.51}$$

The quadratic covariation of $\bar{M}_n^w$ and $\bar{M}_n^y$ is

$$\begin{aligned}\langle \bar{M}_n^w, \bar{M}_n^y \rangle(s) &= \frac{1}{n}\sum_{i=1}^{\lfloor sn \rfloor} -\mathrm{Cov}_{i-1}(dW_i, dY_i) \\ &= \frac{1}{n}\sum_{i=1}^{\lfloor sn \rfloor} pW_{t-1}(1-p+p(1-p)^{n-t})^{W_{t-1}}\left(1-\frac{(1-p)^n}{p(1-p)^n+(1-p)(1-p)^t}\right) \\ &\xrightarrow{\mathbb{P}} \int_0^s \gamma w(x)(1-e^{-\gamma(1-x)})g(x,w(x))dx.\end{aligned} \tag{9.52}$$

Finally, the quadratic covariation of $\bar{M}_n^u$ and $\bar{M}_n^y$ is

$$\begin{aligned}\langle \bar{M}_n^u, \bar{M}_n^y \rangle(s) &= \frac{1}{n}\sum_{i=1}^{\lfloor sn \rfloor} -\mathrm{Cov}_{i-1}(dU_i, dY_i) \\ &= \frac{1}{n}\sum_{i=1}^{\lfloor sn \rfloor}(1-p+p(1-p)^{n-t})^{W_{t-1}}(U_{t-1}-1)(1-(1-p^2)^{W_{t-1}}) \\ &\xrightarrow{\mathbb{P}} \int_0^s \gamma^2 u(x)w(x)g(x,w(x))dx.\end{aligned} \tag{9.53}$$

Using the martingale functional central limit theorem [30], we conclude therefore that $(\bar{M}_n^u, \bar{M}_n^w, \bar{M}_n^y)$ converges in distribution to (W_1, W_2, W_3) where (W_1, W_2, W_3) is described by

$$\begin{aligned}dW_1(s) &= \gamma\sqrt{u(s)w(s)}(dB_1(s) + \sqrt{\gamma u(s)}dB_2(s)) \\ dW_2(s) &= \sqrt{\gamma w(s)}dB_2(s) \\ dW_3(s) &= \sqrt{\gamma w(s)}g(s,w(s))(\sqrt{\gamma u(s)}e^{-\gamma(1-s)}dB_1(s) + (1-e^{-\gamma(1-s)})dB_2(s)) \\ &\quad + \sqrt{g(s,w(s))(1-g(s,w(s))) - \gamma w(s)g(s,w(s))^2(\gamma u(s)e^{-2\gamma(1-s)} + (1-e^{-\gamma(1-s)})^2)}dB_3(s)\end{aligned} \tag{9.54}$$

with B_1, B_2 and B_3 three independent standard Brownian motions.

We now show that $\bar{U}_n(s)$, $\bar{W}_n(s)$ are $\bar{Y}_n(s)$ are stochastically bounded sequences of processes. Stochastic boundedness of $\bar{W}_n(s)$ follows from

$$\begin{aligned}\sup_{s\in[0,1]}|\bar{W}_n(s)| &\leq \sup_{s\in[0,1]}|\bar{M}_n^w(t)| + \gamma\int_0^1 \sup_{s\in[0,x]}|\bar{W}_n(s)|dx \\ &\leq \sup_{s\in[0,1]}|\bar{M}_n^w(t)|e^{\gamma},\end{aligned} \tag{9.55}$$

using Grönwall's inequality and noticing that the martingale is stochastically bounded by the stochastic boundedness criterion for square-integrable martingales [30]. Furthermore,

$$\begin{aligned}\sup_{s\in[0,1]}|\bar{U}_n(s)| &\leq \sup_{s\in[0,1]}|\bar{M}_n^u(t)| + \gamma^2\sup_{s\in[0,1]}|u(s)\bar{W}_n(s)| + \gamma^2\sup_{s\in[0,1]}|w_n(s)|\int_0^1 \sup_{s\in[0,x]}|\bar{U}_n(s)|dx \\ &\leq \left(\sup_{s\in[0,1]}|\bar{M}_n^u(t)| + \gamma^2\sup_{s\in[0,1]}|u(s)\bar{W}_n(s)|\right)\exp(\gamma^2\sup_{s\in[0,1]}|w_n(s)|).\end{aligned} \tag{9.56}$$

Therefore $\bar{U}_n(s)$ is stochastically bounded. Finally, $\bar{Y}_n(s)$ can be shown to be stochastically bounded by

$$\sup_{s\in[0,1]}|\bar{Y}_n(s)| \leq \sup_{s\in[0,1]}|\bar{M}_n^y(t)| + \gamma\sup_{s\in[0,1]}|(1-e^{-\gamma(1-s)})g(s,w(s))\bar{W}_n(s)|. \tag{9.57}$$

Following the same reasoning as in [12], the process must have a subsequence which converges in distribution. Because the limit does not depend on the choice of subsequence, $(\bar{U}_n, \bar{W}_n, \bar{Y}_n)$ converges in distribution to (U, W, Y) where (U, W, Y) is described by

$$\begin{aligned}
dU(s) &= \gamma\sqrt{u(s)w(s)}(dB_1(s) + \sqrt{\gamma u(s)}dB_2(s)) - \gamma^2 w(s)U(s)ds - \gamma^2 u(s)W(s)ds \\
dW(s) &= \sqrt{\gamma w(s)}dB_2(s) - \gamma W(s)ds \\
dY(s) &= \sqrt{\gamma w(s)}g(s, w(s))(\sqrt{\gamma u(s)}e^{-\gamma(1-s)}dB_1(s) + (1 - e^{-\gamma(1-s)})dB_2(s)) \\
&\quad + \sqrt{g(s, w(s))(1 - g(s, w(s))) - \gamma w(s)g(s, w(s))^2(\gamma u(s)e^{-2\gamma(1-s)} + (1 - e^{-\gamma(1-s)})^2)}dB_3(s) \\
&\quad - \gamma(1 - e^{-\gamma(1-s)})g(s, w(s))W(s)ds
\end{aligned} \tag{9.58}$$

with B_1, B_2 and B_3 three independent standard Brownian motions.

To calculate the variance, we will be using theorem 8.5.5 from [31] which is stated as follows.

Lemma: Expectation and variance of SDE
Consider the d-dimensional stochastic differential equation given by

$$dZ(s) = (A(s)Z(s) + a(s))ds + \sum_{i=1}^{d} b_i(s)dB_i(s), \tag{9.59}$$

where $Z(0) = z_0 \in \mathbb{R}^d$, the b_i's are $\mathbb{R}^d$-valued functions and the B_i's are independent standard Brownian motions. Then $Z(t)$ has a normal distribution with mean vector $m(t)$ and covariance matrix $V(t)$, where $m(t)$ and $V(t)$ satisfy the recursion relations

$$\frac{d}{ds}m(s) = A(s)m(s) + a(s), \qquad \frac{d}{ds}V(s) = A(s)V(s) + V(s)A(s)^T + \sum_{i=1}^{d} b_i(s)b_i(s)^T, \tag{9.60}$$

with initial conditions $m(0) = z_0$ and $V(0) = 0$.

For (U, W, Y) this yields

$$\begin{aligned}
A(s) &= \begin{pmatrix} -\gamma^2 w(s) & -\gamma^2 u(s) & 0 \\ 0 & -\gamma & 0 \\ 0 & -\gamma(1 - e^{-\gamma(1-s)})g(s, w(s)) & 0 \end{pmatrix}, \quad a(s) = \begin{pmatrix} 0 \\ 0 \\ 0 \end{pmatrix}, \\
b_1(s) &= \begin{pmatrix} \gamma\sqrt{u(s)w(s)} \\ 0 \\ \gamma\sqrt{u(s)w(s)}e^{-\gamma(1-s)}g(s, w(s)) \end{pmatrix}, \quad b_2(s) = \begin{pmatrix} \sqrt{\gamma^3 u(s)^2 w(s)} \\ \sqrt{\gamma w(s)} \\ \sqrt{\gamma w(s)}(1 - e^{-\gamma(1-s)})g(s, w(s)) \end{pmatrix}, \\
b_3(s) &= \begin{pmatrix} 0 \\ 0 \\ \sqrt{g(s, w(s))(1 - g(s, w(s))) - \gamma w(s)g(s, w(s))^2(\gamma u(s)e^{-2\gamma(1-s)} + (1 - e^{-\gamma(1-s)})^2)} \end{pmatrix}.
\end{aligned} \tag{9.61}$$

If the covariance matrix is denoted by

$$V(s) = \begin{pmatrix} \sigma_{uu}(s) & \sigma_{uw}(s) & \sigma_{uy}(s) \\ \sigma_{uw}(s) & \sigma_{ww}(s) & \sigma_{wy}(s) \\ \sigma_{uy}(s) & \sigma_{wy}(s) & \sigma_{yy}(s) \end{pmatrix}, \tag{9.62}$$

then the variance is

$$\begin{aligned}
\frac{d\sigma_{uu}(s)}{ds} &= -2\gamma^2 w(s)\sigma_{uu}(s) + \gamma^2 u(s)((1+\gamma u(s))w(s) - 2\sigma_{uw}(s)) \\
\frac{d\sigma_{uw}(s)}{ds} &= -\gamma(1+\gamma w(s))\sigma_{uw}(s) + \gamma^2 u(s)(w(s) - \sigma_{ww}(s)) \\
\frac{d\sigma_{ww}(s)}{ds} &= -2\gamma\sigma_{ww}(s) + \gamma w(s) \\
\frac{d\sigma_{wy}(s)}{ds} &= -\gamma\sigma_{wy}(s) + \gamma(1-e^{-\gamma(1-s)})g(s,w(s))(w(s) - \sigma_{ww}(s)) \\
\frac{d\sigma_{uy}(s)}{ds} &= -\gamma^2 w(s)\sigma_{uy}(s) - \gamma(1-e^{-\gamma(1-s)})g(s,w(s))\sigma_{uw}(s) + \gamma^2 u(s)(w(s)g(s,w(s)) - \sigma_{wy}(s)) \\
\frac{d\sigma_{yy}(s)}{ds} &= -2\gamma(1-e^{-\gamma(1-s)})g(s,w(s))\sigma_{wy}(s) + g(s,w(s))(1-g(s,w(s))).
\end{aligned} \tag{9.63}$$

The differential equations can be solved and simplified to

$$\begin{aligned}
\sigma_{uu}(s) &= \exp(2\beta\gamma e^{-\gamma s}) \int_0^s \exp(-2\beta\gamma e^{-\gamma x})\gamma^2 u(x)((1+\gamma u(x))w(x) - 2\sigma_{uw}(x))dx, \\
\sigma_{uw}(s) &= \exp(\gamma(\beta e^{-\gamma s} - s)) \int_0^s \exp(-\gamma(\beta e^{-\gamma x} - x))\gamma^2 u(x)(w(x) - \sigma_{ww}(x))dx, \\
\sigma_{ww}(s) &= \exp(-2\gamma s) \int_0^s \exp(2\gamma x)\gamma w(x)dx = \beta e^{-\gamma s}(1-e^{-\gamma s}), \\
\sigma_{wy}(s) &= \exp(-\gamma s) \int_0^s \exp(\gamma x)\gamma(1-e^{-\gamma(1-x)})g(x,w(x))(w(x) - \sigma_{ww}(x))dx, \\
\sigma_{uy}(s) &= \exp(\beta\gamma e^{-\gamma s}) \int_0^s \exp(-\beta\gamma e^{-\gamma x})(-\gamma(1-e^{-\gamma(1-x)})g(x,w(x))\sigma_{uw}(x) \\
&\quad + \gamma^2 u(x)(w(x)g(x,w(x)) - \sigma_{wy}(x)))dx, \\
\sigma_{yy}(s) &= \int_0^s -2\gamma(1-e^{-\gamma(1-x)})g(x,w(x))\sigma_{wy}(x) + g(x,w(x))(1-g(x,w(x)))dx.
\end{aligned} \tag{9.64}$$

9.6 Hitting time distribution

With the variance of the three processes known, the final step will consist of obtaining the distribution of the hitting time, the time at which the process $u_n(s)$ hits zero. Furthermore, the asymptotic distribution of the Y process at the hitting time will also be determined as this is used in the decomposed random intersection graph. Define

$$v_n = (u_n, w_n, y_n), \tag{9.65}$$

where $v_n \xrightarrow{\mathbb{P}} v$ with $v = (u, w, y)$. Moreover, define

$$\bar{V}_n(s) = \sqrt{n}(v_n(s) - v(s)) = (\bar{U}(s), \bar{W}(s), \bar{Y}(s)), \tag{9.66}$$

where $\bar{V}_n \xrightarrow{D} V$ with $V = (U, W, Y)$. Now note that

$$v(s) = v_0 + \int_0^s F(v(x))dx, \tag{9.67}$$

where $v_0 = (1, \beta, 0)$ and

$$F(u, w, y) = \begin{pmatrix} -1 - \gamma^2 uw \\ -\gamma w \\ \exp(\beta\gamma e^{-\gamma} - \gamma w) \end{pmatrix}. \tag{9.68}$$

Theorem 12.4.1 from [21], the hitting time distribution theorem, is stated as follows.

Lemma: Hitting time distribution
Let h be continuously differentiable on $\mathbb{R}^d$. Let v_n and v be defined as above with $h(v(0)) > 0$. Let

$$\phi_n = \inf\{s : h(v_n(s)) \leq 0\} \tag{9.69}$$

and

$$\phi = \inf\{s : h(v(s)) \leq 0\}. \tag{9.70}$$

Suppose $\phi < \infty$ and

$$\nabla h(v(\phi)) \cdot F(v(\phi)) < 0. \tag{9.71}$$

Then

$$\sqrt{n}(\phi_n - \phi) \xrightarrow{D} -\frac{\nabla h(v(\phi)) \cdot V(\phi)}{\nabla h(v(\phi)) \cdot F(v(\phi))} \tag{9.72}$$

and

$$\sqrt{n}(v_n(\phi_n) - v(\phi)) \xrightarrow{D} V(\phi) - \frac{\nabla h(v(\phi)) \cdot V(\phi)}{\nabla h(v(\phi)) \cdot F(v(\phi))} F(v(\phi)). \tag{9.73}$$

In our case, let $h(u, w, y) = u$. Then $h(v(0)) = 1 > 0$ and $\nabla h(v(\phi)) \cdot F(v(\phi)) = -1 < 0$. Notice that with this definition of h, the fraction of the number of activated vertices in the jamming limit is denoted by ϕ_n. Thus

$$\sqrt{n}(\phi_n - \phi) \xrightarrow{D} U(\phi), \tag{9.74}$$

as $n \to \infty$. Moreover,

$$\sqrt{n}(y_n(\phi_n) - y(\phi)) \xrightarrow{D} Y(\phi) + U(\phi)\exp(\beta\gamma e^{-\gamma} - \gamma w(\phi)) = Y(\phi) + U(\phi)y'(\phi), \tag{9.75}$$

as $n \to \infty$. This proves the central limit theorem for a random intersection graph.

■

References

[1] D. Jaksch et al. “Fast quantum gates for neutral atoms”. In: *Physical Review Letters* 85.10 (2000), p. 2208.

[2] Mark Saffman, Thad G. Walker, and Klaus Mølmer. “Quantum information with Rydberg atoms”. In: *Reviews of Modern Physics* 82.3 (2010), p. 2313.

[3] Daniel Comparat and Pierre Pillet. “Dipole blockade in a cold Rydberg atomic sample”. In: *JOSA B* 27.6 (2010), A208–A232.

[4] Yevhen Miroshnychenko et al. “Observation of collective excitation of two individual atoms in the Rydberg blockade regime”. In: *Nature Physics* 5.2 (2009), p. 115.

[5] Daniel Barredo et al. “Demonstration of a strong Rydberg blockade in three-atom systems with anisotropic interactions”. In: *Physical Review Letters* 112.18 (2014), p. 183002.

[6] Peter Schauß et al. “Observation of spatially ordered structures in a two-dimensional Rydberg gas”. In: *Nature* 491.7422 (2012), p. 87.

[7] Leonard Mandel. “Sub-Poissonian photon statistics in resonance fluorescence”. In: *Optics Letters* 4.7 (1979), pp. 205–207.

[8] Christoph S. Hofmann et al. “Sub-Poissonian statistics of Rydberg-interacting dark-state polaritons”. In: *Physical Review Letters* 110.20 (2013), p. 203601.

[9] Matthieu Viteau et al. “Cooperative excitation and many-body interactions in a cold Rydberg gas”. In: *Physical Review Letters* 109.5 (2012), p. 053002.

[10] Jaron Sanders, Matthieu Jonckheere, and Servaas Kokkelmans. “Sub-Poissonian statistics of jamming limits in ultracold Rydberg gases”. In: *Physical Review Letters* 115.4 (2015), p. 043002.

[11] Francis Robicheaux and J.V. Hernández. “Many-body wave function in a dipole blockade configuration”. In: *Physical Review A* 72.6 (2005), p. 063403.

[12] Souvik Dhara, Johan S.H. van Leeuwaarden, and Debankur Mukherjee. “Corrected mean-field model for random sequential adsorption on random geometric graphs”. In: *arXiv preprint arXiv:1611.05019* (2016).

[13] Mathew D. Penrose and Joseph E. Yukich. “Limit theory for random sequential packing and deposition”. In: *Annals of Applied probability* (2002), pp. 272–301.

[14] Jian-Sheng Wang. “A fast algorithm for random sequential adsorption of discs”. In: *International Journal of Modern Physics C* 5.04 (1994), pp. 707–715.

[15] Ronald Dickman, Jian-Sheng Wang, and Iwan Jensen. “Random sequential adsorption: Series and virial expansions”. In: *The Journal of Chemical Physics* 94.12 (1991), pp. 8252–8257.

[16] Edward G. Coffman Jr. et al. “Packing random intervals on-line”. In: *Algorithmica* 22.4 (1998), pp. 448–476.

[17] Alfred Rényi. “On a one-dimensional random space-filling problem”. In: *MTA Mat Kut. Int. Kzl* (1958), pp. 109–127.

[18] Paul Erdös and Alfréd Rényi. “On random graphs, I”. In: *Publicationes Mathematicae (Debrecen)* 6 (1959), pp. 290–297.

[19] Paola Bermolen, Matthieu Jonckheere, and Jaron Sanders. “Scaling limits for exploration algorithms”. In: *arXiv preprint arXiv:1504.02438* (2015).

[20] Colin McDiarmid. “Colouring random graphs”. In: *Annals of Operations Research* 1.3 (1984), pp. 183–200.

[21] Stewart N. Ethier and Thomas G. Kurtz. *Markov processes: characterization and convergence*. Vol. 282. John Wiley & Sons, 2009.

[22] Joona Karjalainen and Lasse Leskelä. “Moment-based parameter estimation in binomial random intersection graph models”. In: *International Workshop on Algorithms and Models for the Web-Graph*. Springer. 2017, pp. 1–15.

[23] Michał Karoński, Edward R. Scheinerman, and Karen B. Singer-Cohen. "On random intersection graphs: The subgraph problem". In: *Combinatorics, Probability and Computing* 8.1-2 (1999), pp. 131–159.

[24] Dudley Stark. "The vertex degree distribution of random intersection graphs". In: *Random Structures & Algorithms* 24.3 (2004), pp. 249–258.

[25] Maria Deijfen and Willemien Kets. "Random intersection graphs with tunable degree distribution and clustering". In: *Probability in the Engineering and Informational Sciences* 23.4 (2009), pp. 661–674.

[26] James Allen Fill, Edward R. Scheinerman, and Karen B. Singer-Cohen. "Random intersection graphs when m=omega(n): An equivalence theorem relating the evolution of the G(n, m, p) and G(n, p) models". In: *Random Struct. Algorithms* 16.2 (2000), pp. 156–176.

[27] Josep Díaz et al. "On the relation between graph distance and Euclidean distance in random geometric graphs". In: *Advances in Applied Probability* 48.3 (2016), pp. 848–864.

[28] Ioannis Karatzas and Steven Shreve. *Brownian motion and stochastic calculus*. Vol. 113. Springer Science & Business Media, 2012.

[29] Robert Liptser and Albert Nikolaevich Shiryayev. *Theory of martingales*. Vol. 49. Springer Science & Business Media, 2012.

[30] Guodong Pang, Rishi Talreja, Ward Whitt, et al. "Martingale proofs of many-server heavy-traffic limits for Markovian queues". In: *Probability Surveys* 4 (2007), pp. 193–267.

[31] Ludwig Arnold. "Stochastic differential equations". In: *Proceedings of the International Symposium MTNS-89, Volume I* (1974).